1965

A second study of homogeneous nucleation of water vapor in helium

Raymond J. Schmitt

A SECOND STUDY OF HOMOGENEOUS NUCLEATION OF WATER VAPOR IN HELIUM

BY

RAYMOND J. SCHMITT

AN

ABSTRACT

submitted to the faculty of the

UNIVERSITY OF MISSOURI AT ROLLA

in partial fulfillment of the requirements for the

Degree of

MASTER OF SCIENCE, PHYSICS MAJOR

Rolla, Missouri

1965

A SECOND STUDY OF HOMOGENEOUS NUCLEATION OF WATER VAPOR IN HELIUM

Absolute homogeneous nucleation rates in a supersaturated mixture of water vapor and helium are measured using a long sensitive time expansion chamber and a method devised by Kassner and Allard. A pulse technique is employed to produce the nucleation in an effort to suppress disturbing influences of vapor depletion and droplet growth. The time-varying nature of the supersaturation during the nucleation pulse is taken into account by an integration over the pulse. Observed and theoretically predicted droplet concentrations are related by an assumed nucleation rate law which is adjusted until the total droplet populations predicted by integration of the assumed law agree with experiment to within ±10%. The empirical nucleation rate law that results from this analysis is compared to the theoretical results of Becker and Döring, Frenkel and Courtney. The classical calculation of Becker and Döring is presented in detail.

A SECOND STUDY OF HOMOGENEOUS NUCLEATION OF WATER VAPOR IN HELIUM

BY

RAYMOND J. SCHMITT

A

THESIS

submitted to the faculty of the

UNIVERSITY OF MISSOURI AT ROLLA

in partial fulfillment of the requirements for the

Degree of

MASTER OF SCIENCE, PHYSICS MAJOR

Rolla, Missouri

1965

Approved by

J. L. Kassner Jr. (advisor) W. J. James

Louis D. Grand. Ralph E. Lee

ACKNOWLEDGEMENTS

The author wishes to thank his advisor, Dr. James L. Kassner, Jr., for the encouragement, advice and assistance extended by him during the course of this research.

Thanks are due to the author's co-researchers, Mr. Louis B. Allen, Mr. Ronald Dawbarn, Mr. Michael A. Grayson, and Mr. Donald L. Packwood, for their help in setting up the equipment for this study. Gratitude is also expressed to Mr. Daniel Eppelsheimer, to Mr. Carl Lund and to Mr. Robert P. Madding for their contributions to this research. Thanks are due to Mr. Lee N. Anderson of the Mechanical Engineering Department for his fine machine work.

Finally, thanks are due to Lt. Edward F. Allard, United States Army, who accomplished the original nucleation studies here at UMR and who assisted the author in learning to operate the apparatus.

This research was supported by the Atmospheric Sciences Section of the National Science Foundation, NSF Grant GP-2893.

TABLE OF CONTENTS

LIST OF FIGURES

LIST OF TABLES

LIST OF PLATES

CHAPTER I

STATEMENT OF THE PROBLEM

1. Introduction. Condensation of a vapor under conditions of mild supersaturations which are obtained in expansion chambers is fundamental toward an understanding of a large number of nucleation phenomena which have been observed in the solid, liquid and gaseous phases. The formation of a metal oxide in an expansion nozzle, recrystallization in steel, the formation of water droplets during cloud formation or in aircraft "contrails" are examples of nucleation phenomena. The term "nucleation" refers to the generation within a bulk parent phase of minute clusters of a new phase. The condensation of liquid water droplets from a supersaturated mixture of helium and water vappr is the specific form of nucleation which is studied here. A modified Blackett-type expansion chamber is used to produce a condition of vapor supersaturation by adiabatic cooling of the gas-vapor mixture. The concentration of water droplets which nucleate and grow to visible size will be measured as a function of the supersaturation and the sensitive time of the chamber. Nucleation rates can then be deduced from knowledge of the droplet concentrations and the sensitive times.

2. Homogeneous Nucleation.[1] Dropwise condensation falls into two categories: homogeneous nucleation and

heterogeneous nucleation. Homogeneous nucleation refers to those condensation processes in which clustering involves only molecules of the parent phase and is not catalyzed by impurities or foreign particles. Clusters of water vapor molecules serve as centers of condensation, or nuclei, in the present studies. Whether or not a phase transition will take place in a pure vapor depends on whether or not nucleation of the new phase can occur. In the absence of all foreign surfaces or particles (heterogeneous nucleants), phase transition does not occur until some finite degree of supersaturation or supercooling has developed. Since condensation occurs rapidly once macroscopic particles of the new phase have nucleated, nucleation is often a bottleneck to condensation.

A vapor is said to be supersaturated when the vapor density at temperature T exceeds the normal saturated vapor density at that temperature. The supersaturation, S, is defined by

$$S = \rho/\rho_{\infty}, \qquad (1\text{-}1)$$

where ρ is the actual vapor density at temperature T and ρ_{∞} is the equilibrium vapor density over a plane surface of the liquid at the same temperature. Supersaturation is also defined in terms of vapor pressures as p/p_{∞}, where p is the actual vapor pressure at temperature T and p_{∞} is the equilibrium vapor pressure over a plane surface of the liquid at the same temperature. When water vapor is cooled rapidly in an adiabatic expansion, ρ can be

several times larger than p_∞, hence the term "supersaturation."

In the saturated state an equilibrium distribution of various sizes of clusters is postulated to exist in the vapor. Simple inelastic binary collisions are assumed to give rise to this distribution. The Gibbs free energy of the clusters is distributed according to the familiar Boltzmann distribution of classical statistical mechanics. The number of clusters of g molecules each (g-mers) per unit volume in the distribution is

$$n_g = n_1 \exp(-\Delta F_g/kT), \qquad (1\text{-}2)$$

where n_1 is the number of monomers (single vapor molecules) per unit volume, ΔF_g is the excess Gibbs free energy of the g-mer over that of the plane liquid, K is the Boltzmann constant and T is the absolute temperature of the system (which is assumed to be the temperature of the clusters in the equilibrium distribution).

The free energy of the g-mer distribution is characterized by a maximum occurring at a certain value of g given by

$$g^* = \left[\frac{2a\sigma}{3kT\ln S}\right]^3 \qquad (1\text{-}3)$$

where a is the mole fraction of the monomer, σ is the surface tension of the bulk liquid and S is the supersaturation. Since the total number of clusters is presumed to be small when compared to n_1, the monomer concentration, the mole fraction, a, is taken as unity. Clusters of size g^* are called "nuclei." The nuclei are in

metastable equilibrium with the vapor and the chance acquisition of another vapor molecule causes them to become free-growing. An idea of how g* varies with S can be obtained from Table I.[1]

TABLE I

CRITICAL NUCLEI SIZES

$T = 0^{\circ}C.$									
S	2	3	4	5	6	7	8	9	10
g*	695	174	87	55	40	31	26	22	20

The existence of g* is a consequence of the assumptions made for the Gibbs free energy of the g-mer, ΔF_g. A tiny spherical liquid droplet in equilibrium with its vapor at temperature T has a larger Gibbs free energy than the plane liquid. It is common practice to write the increase in the Gibbs free energy of the system due to the formation of a single, spherical g-mer from g vapor molecules as the sum of a surface and of a volume contribution,

$$\Delta F_g = (F_L - F_V)g + 4\pi r^2\sigma \qquad (1\text{-}4)$$

where F_V and F_L are the free energies per molecule of the vapor and liquid phases respectively and r is the radius of the g-mer. The first term is the volume contribution while the second term represents the contribution to the free energy of the droplet due to the surface. For an isobaric-isothermal formation of the g-mer from g vapor molecules we have

$$g(F_L - F_V) = -(4/3)\pi r^3 \rho RT \ln S \qquad (1\text{-}5)$$

where ρ is the density of the liquid phase and R is the universal gas constant. The assumption that this process is isobaric implies that only an insignificant amount of vapor is condensed in the formation of the g-mers. Hence the pressure of the vapor remains constant. The assumption that the process is isothermal implies that the heating of the vapor by the condensing droplets is negligible. Both of these assumptions are unrealistic and are done away with in more sophisticated developments of nucleation theory.[2,3]

Equation (1-4) becomes

$$\Delta F_g = 4\pi r^2 \sigma - (4/3)\pi r^3 \rho RT \ln S \qquad (1\text{-}6)$$

which can be written in terms of g since

$$mg = (4/3)\pi r^3 \rho \qquad (1\text{-}7)$$

where m is the mass of one water molecule. Equation (1-6) has a maximum, ΔF_g^*, for g^* given by eq. (1-3). Droplets smaller in size than g^* tend to have a larger vapor pressure than the nucleus due to their greater radius of curvature. Thus the vapor is unsaturated with respect to the former and saturated with respect to the latter. Similarly a droplet larger in size than g^* tends to have a smaller vapor pressure than the nucleus and thus the surrounding vapor is supersaturated with respect to these larger droplets. Clusters whose sizes are less than g^* will tend to evaporate while those clusters larger in size than g^* will tend to grow larger through condensation of the

vapor. However, eq. (1-2) indicates that the population of clusters larger in size than g* is vanishingly small for the saturated vapor (S = 1). This means that spontaneous formation of droplets of liquid in a saturated vapor is prevented by a free energy barrier (or activation energy barrier) of height ΔF_g^* which is so great, i.e. g* is so large, that dropwise condensation is not noticable.

As the supersaturation, S, increases, g* decreases and n_g^* increases. For S = 4.0 and T = 0°C, g* is 87 molecules and n_g^* is approximately 6.0×10^{-6} nuclei/cm^3 for water. For S = 5.0 and T = 0°C, g* is 55 molecules and n_g^* has increased to approximately 10 nuclei/cm^3. Evidence of an increase in droplet concentrations with increasing supersaturation is easily obtained in expansion chamber experiments. However, there has been some disagreement among researchers over the precise supersaturation level at which condensation becomes noticable. This point will be discussed at length below. It is well to point out now that the liquid-drop theory of condensation which has been outlined in the preceeding pages is not amenable to experimental test using an expansion chamber since cluster populations cannot be measured directly with this device. However, there is the possibility of making accurate determinations of droplet concentrations, supersaturations and temperatures with an expansion chamber. From such data homogeneous nucleation rates may be deduced

and compared with theory.

3. Homogeneous Nucleation Rate. From the preceeding discussion it is evident that homogeneous nucleation is an intrinsically probabilistic event. The kinetic theory of gases can be employed to predict nucleation rates in supersaturated vapors.[1,2,4,5,6,7] The homogeneous nucleation rate is the number of nuclei per cm^3 per second produced in a vapor at temperature T and supersaturation S. A review of some of the important nucleation rate theories will be given in chapter II. Most of these theories begin with the following basic assumptions:

a. Simple inelastic binary collision is the mechanism by which clusters increase in size.

b. The clusters are assumed to possess the properties of the bulk liquid phase.

c. The growth of a g-mer into a (g + 1)-mer is considered to be very similar to a chemical reaction with characteristic forward and reverse reaction rates. The law of mass action is freely used to describe these reaction rates in terms of monomer and cluster concentrations.

d. Most nucleation rate theories are strictly equilibrium theories in which a steady-state nucleation rate is deduced from considerations of detailed microscopic balancing conditions for dynamic equilibrium between g-mers and (g + 1)-mers.[7] In the equilibrium condition the cluster populations remain

constant while a drift from smaller to larger cluster sizes occurs.

e. The number of vapor molecules present in the system is assumed to be much greater than the total number of clusters of all sizes.

f. Accommodation coefficients for growth and dissociation are introduced to account for the probability that a vapor molecule will stick when it collides with a cluster and that a vapor molecule will leave a cluster respectively. Most authors guess at these values.

4. Critical Supersaturation. The homogeneous nucleation process is characterized by an exceedingly rapid increase in the nucleation rate with increasing supersaturation varying from a few drops per cm^3 per second at a supersaturation of 4.9 to several thousand drops per cm^3 per second at a supersaturation of 5.2. The dramatic increase in droplet concentration with a slight change in supersaturation was noticed first by Wilson.[8] In a series of classic experiments he demonstrated the existence of two critical supersaturations, one at S = 4.2, the ion limit, for condensation on ions (heterogeneous nucleation) and one at S = 8.0, the fog limit, for supposed homogeneous nucleation. Since that time most experimental endeavors with expansion chambers have been directed toward investigation of these critical supersaturation levels as functions of temperature, pressure and nature of the vapor.[9,14]

In view of the experimental evidence tending to support the idea of critical supersaturations, the homogeneous nucleation process in vapors came to be considered an on-off phenomenon. In other words, S has to be larger than the critical supersaturation before nucleation can proceed and droplets can be observed. It is possible to show by means of refined expansion chamber techniques to be described below that the nucleation process is not, strictly speaking, on-off. It is true that the nucleation process can be halted by lowering the supersaturation sufficiently. However, the nucleation process does not cut off so quickly that it can in reality be considered an on-off process.

The idea of a fog limit is a rather hazy concept at best since different researchers use different droplet concentrations as the fog limit. Some use one droplet per cm^3 while others use 100 or more droplets per cm^3 as the criterion. Used in this way, the notion of a fog limit has very little worth for nucleation studies. The fog limit, or critical supersaturation for homogeneous nucleation, in effect is a measure of the sensitivity of the method utilized to determine droplet concentrations. It is a measure of the lowest possible droplet concentrations above the normal background fog density of the chamber that can be measured with a given expansion chamber using a given technique for observing the droplets.[12] Obviously a chamber with a large sensitive volume will be

able to yield accurate measurements of small droplet concentrations provided low background concentrations are possible. Our chamber and a high resolution photographic technique developed in this laboratory can accurately provide background droplet concentrations of less than one droplet per 40 cm^3 even when the previous expansions yield high droplet concentrations, say, 50 - 100 droplets/cm^3. In the following pages the terms "critical supersaturation" and "fog limit" will refer to the supersaturation 4.300 corresponding to the limit of resolving power of the chamber used in these researches. At S = 4.300 background nucleation begins to severely alter the empirical nucleation rate which is deduced from the observed droplet concentration.

The mention made above of background brings up the question "What provides the background nucleation for these experiments and what can one do to decrease it"? Since these experiments are homogeneous nucleation studies, the background will consist of heterogeneous nucleation. If one were considering heterogeneous nucleation, then the background would be provided by the homogeneous condensation. It is imperative that one be able to distinguish homogeneous nucleation from background nucleation if homogeneous nucleation rates are to be precisely determined. In a carefully purified, dust-free chamber, ions and re-evaporation nuclei are the most important heterogeneous nucleants.

Ionizing particles leave a trail of charged nucleation centers which condense vapor to form the familiar cloud chamber tracks.[13] Heterogeneous nucleation in the form of such tracks is not difficult to identify and causes no problem in these experiments. But tracks will diffuse if given sufficient time and the charged droplets from these tracks will blend in with the homogeneous nucleation and alter the droplet count in an unpredictable way. In these experiments on homogeneous nucleation rates, such background heterogeneous nucleation is suppressed by establishing a large electrostatic field, called the clearing field, in the sensitive volume of the chamber. The water in the bottom of the chamber acts as one electrode and a set of wires near the top of the chamber is the other electrode. Fields of 100-200 volts/cm are commonly used and are quite effective in cleaning the chamber of this kind of background condensation even though the prevailing supersaturations can be much higher than the ion limit.

The problem of re-evaporation nuclei is discussed in chapter III. A method for reducing this troublesome source of background will be presented there.

5. Droplet Growth. The subsequent growth of the condensation nuclei to visible size comprises the second stage of the dropwise condensation process. An investigation of droplet growth laws is not contemplated in this paper. Yet the processes of homogeneous nucleation and

droplet growth are so inter-connected that a few words on the latter phenomenon are in order here. From one point of view the experiments performed by this writer represent attempts to uncouple homogemeous nucleation from the effects of droplet growth. The method used here for determining homogeneous nucleation rates without having to simultaneously verify the droplet growth law will be described below.

Droplet growth must be taken into account in expansion chamber determinations of nucleation rates insofar as the process of growth affects the observed nucleation rates. Two effects of droplet growth combine to alter the initial nucleation rate established by a rapid, quasi-adiabatic expansion of the vapor. First, the nuclei grow at the expense of the surrounding vapor which is rapidly depleted near the growing droplets. The vapor density in these "dead" spaces surrounding the growing droplets is rapidly lowered and so S is lower in these regions. Not only is the density of nuclei forming per unit time in the dead spaces greatly reduced, but also nuclei which do form there will grow more slowly to visible size due to the vapor depletion. Thus measurement of the nucleation rate, which depends on visible droplet counts, cannot be accurately made if the total concentration of droplets becomes so large that, say, 100 droplets per cm^3 are all competing for what vapor is available. Secondly, the latent heat of condensation warms the vapor near the

growing droplets and reduces the supersaturation there, lowering the nucleation rate even more. Typically, the effects of vapor depletion become noticable within 0.05 seconds for given initial supersaturations in fast cloud chambers.

The nucleation process occurs over a wide range of supersaturations and, hence, over a wide range of rates, due, in part, to vapor depletion effects. The possibility of accurately correlating a true nucleation rate with a definite supersaturation from data taken in a single cloud chamber expansion is remote. One is placed in the position of having to simultaneously verify the nucleation rate law and the droplet growth law if an attempt is made to correct for vapor depletion by computational means.[2] Clearly an experimental method is required by which the effects of droplet growth on the homogeneous nucleation rate can be eliminated as much as possible. Kassner and Allard[12] have developed such a method and the specialized equipment required for its use.

6. Sensitive Time. The sensitive time of an expansion chamber is the time interval during which nuclei of condensation are being produced in the vapor in observable amounts. Hence, the sensitive time depends on the sensitivity of the observational technique employed in droplet count determinations. A condition of supersaturation is produced by rapid, adiabatic cooling of the gas-vapor mixture (the sensitive volume). The expansion is made

rapidly (approximately 0.13 sec) so the sensitive time can be considered to begin near the end of the expansion. Homogeneous nucleation and droplet growth are observed when S exceeds the fog limit. In chambers operating in the conventional manner, nucleation proceeds until vapor depletion and heating effects from the chamber walls and from the condensing vapor lower S below the fog limit. At this point the sensitive time ends. Droplets nucleated during the sensitive time will continue to grow until vapor depletion and wall heating effects cause evaporation to predominate over condensation. When the nucleation process cuts off in this manner, the sensitive time is said to be naturally terminated.

Heating of the sensitive volume by conduction from the walls of the chamber has a pronounced effect on the sensitive time. Conduction of heat in gases is so slow that ordinarily one would not expect heating effects to be noticable near the center of the chamber until a second or more after the beginning of the expansion.[15] However, a mechanism does exist by which heating effects are transmitted throughout the sensitive volume immediately after the expansion. A thin layer of gas close to the walls is heated very rapidly by conduction and expands, thus compressing the entire sensitive volume. The supersaturation decreases since the temperature of the sensitive volume is increasing. The nucleation rate drops until finally nucleation cuts off and the sensitive time

ends. A continuing expansion technique has been developed in this laboratory which enables one to compensate for compressive heating effects. A discussion will be postponed until chapter III.

Control of the sensitive time is essential in homogeneous nucleation experiments. Kassner and Allard have developed a method for artificially terminating the sensitive time in an effort to experimentally correct homogeneous nucleation rate measurements for effects of droplet growth. A short sensitive time of approximately 0.03 sec. duration can be produced during which time the pressure and, hence, the supersaturation can be accurately determined from oscillograph recordings. With knowledge of S as a function of time and an assumed nucleation rate law, a prediction of the concentration of droplets can be made. Photographic determination of actual droplet concentrations yield empirical results which can be compared with the predicted droplet concentration. The nucleation rate law is adjusted until agreement is obtained. This method for determining the homogeneous nucleation rate law is discussed fully in chapter IV.

CHAPTER II

REVIEW OF LITERATURE

Theory

A vast literature exists on homogeneous condensation of vapors in expansion chambers. Most of the theoretical treatments of the homogeneous nucleation phenomenon are steady-state theories which predict a steady-state nucleation rate as a function of supersaturation. The specific problem to which all nucleation theories are directed is to predict the rate of formation of nuclei per unit volume in a closed system containing a supersaturated vapor, clusters of a new phase and an inert gas. Almost all nucleation theories use the liquid-drop model for deriving the kinetic and thermodynamic properties of the clusters and of the critical nucleus.

1. Liquid-Drop Thermodynamics.[7] Kelvin[13] deduced the thermodynamic criterion for equilibrium between a g-mer and its vapor,

$$RT\ln S = 2M\sigma/\rho r, \qquad (2\text{-}1)$$

where r = radius of the g-mer,

M = molecular weight of the liquid,

ρ = liquid density,

σ = surface tension,

S = supersaturation.

Equation (2-1) is developed by the same arguments that led to eq. (1-6). In fact, equation (2-1) is identical to eq. (1-3) if eq. (1-7) is used to replace r by g. From equations (1-4) and (1-7) we have

$$\Delta F_g = (F_L - F_V)g + 4\pi r^2\sigma. \tag{2-2}$$

When a droplet is size g*, it is in equilibrium with the surrounding vapor, but the equilibrium is metastable since ΔF_g has a maximum at g = g* instead of a minimum (cf. fig. 1). The equilibrium condition is $d(\Delta F_g)/dg = 0$, which is satisfied when

$$F_L - F_V = -2/3\ mg^{-1/3} = -(8\pi\sigma r^2)/3g, \tag{2-3}$$

where m is a constant such that

$$mg^{2/3} = 4\pi r^2\sigma.$$

Since g is related to r by

$$g = (4\pi r^3 N_o \rho)/3M,$$

where N_o is Avogadro's number, we have

$$F_V - F_L = (2M\sigma)/(N_o\rho r). \tag{2-4}$$

Consider now an isothermal process in which the vapor pressure changes by dp. Then,

$$\begin{aligned} dF_V &= vdp \\ dF_L &= Vdp, \end{aligned} \tag{2-5}$$

where v is the volume per molecule in the vapor phase and V is the volume per molecule in the liquid phase. Then

$$d(F_V - F_L) = (v - V)dp \simeq kTdp/p, \tag{2-6}$$

since V<<v. Integrating from p_∞, the saturation vapor pressure to p, the vapor pressure of the droplet, yields

$$F_V - F_L = kT\ln(p/p_\infty) = kT\ln S. \tag{2-7}$$

Hence, for equilibrium the result is,

$$kT\ln S = 2/3\ mg^{-1/3} = 2M\sigma/\rho r, \qquad (2\text{-}8)$$

which is the Kelvin equation.

According to eq. (2-2) stable equilibrium occurs for $g = 0$. But there is always a small probability that the system will be found in a non-equilibrium state, i.e. $g > 0$. The probability[5] of finding a non-equilibrium state of energy ΔF_g is proportional to $\exp(-\Delta F_g/kT)$. Using equation (2-2) for ΔF_g, the probability of finding the chamber containing a liquid droplet of any specified size may be calculated. The most probable distribution of g-mers will then be a Boltzmann distribution, eq. (1-2). From figure 2 it can be seen that the critical nucleus is the cluster size in the smallest concentration. This feature makes nucleation the bottleneck in the condensation process. Figure 2 also shows that eq. (1-2) cannot be correct for $S > 1$ since n_g becomes greater than n_1 for large g, an obvious impossibility in a real system. One must resort to the kinetic theory of gases in order to determine the true distribution curve.

2. Liquid-Drop Kinetics.[2] The nucleation rate is defined as

$$J = K_1 n_g^*, \qquad (2\text{-}9)$$

where

$$n_g^* = n_1 \exp(-\Delta F_g^*/kT)$$
$$= n_1 \exp\left[-(16\pi\sigma^3 M^2)/3(\rho RT\ln S)^2 kT\right]$$

and K_1 is a kinetic coefficient with units sec^{-1}. Equation (2-9) is useful because of the singular behavior

of the exponential factor. This factor is extremely sensitive to changes in S, increasing from a very small value to a very large value for a comparatively small change in S (cf. fig. 3). Such behavior is in qualitative agreement with expansion chamber results. The point at which this increase occurs represents a critical limit of metastability at which the mother phase can no longer exist.[16,17,18] The determination of the critical supersaturation for which this increase in J occurs has been the object of most cloud chamber researches since Wilson's original experiments.[8,14,20] Only Frey[11] has seriously undertaken expansion chamber studies in an effort to find a nucleation rate law which could be compared to eq. (2-9). His researches are discussed below. As it stands eq. (2-9) is incomplete since the kinetic coefficient, K_1, has not yet been specified. The evaluation of K_1 is then the goal of the nucleation rate theories.

The classical liquid drop theory of nucleation rests on the assumption that nucleation rates can be calculated from relatively simple kinetic and thermodynamic considerations. The first fragments of the condensed phase are assumed to be well defined liquid droplets possessing the bulk properties of a volume of the liquid with a plane surface. The nucleation rate theories of Becker and Döring,[4] Frenkel,[5] and Courtney[2] rely on the liquid drop hypothesis. The experimentally observed rate of condensation is very sensitive to the supersaturation and

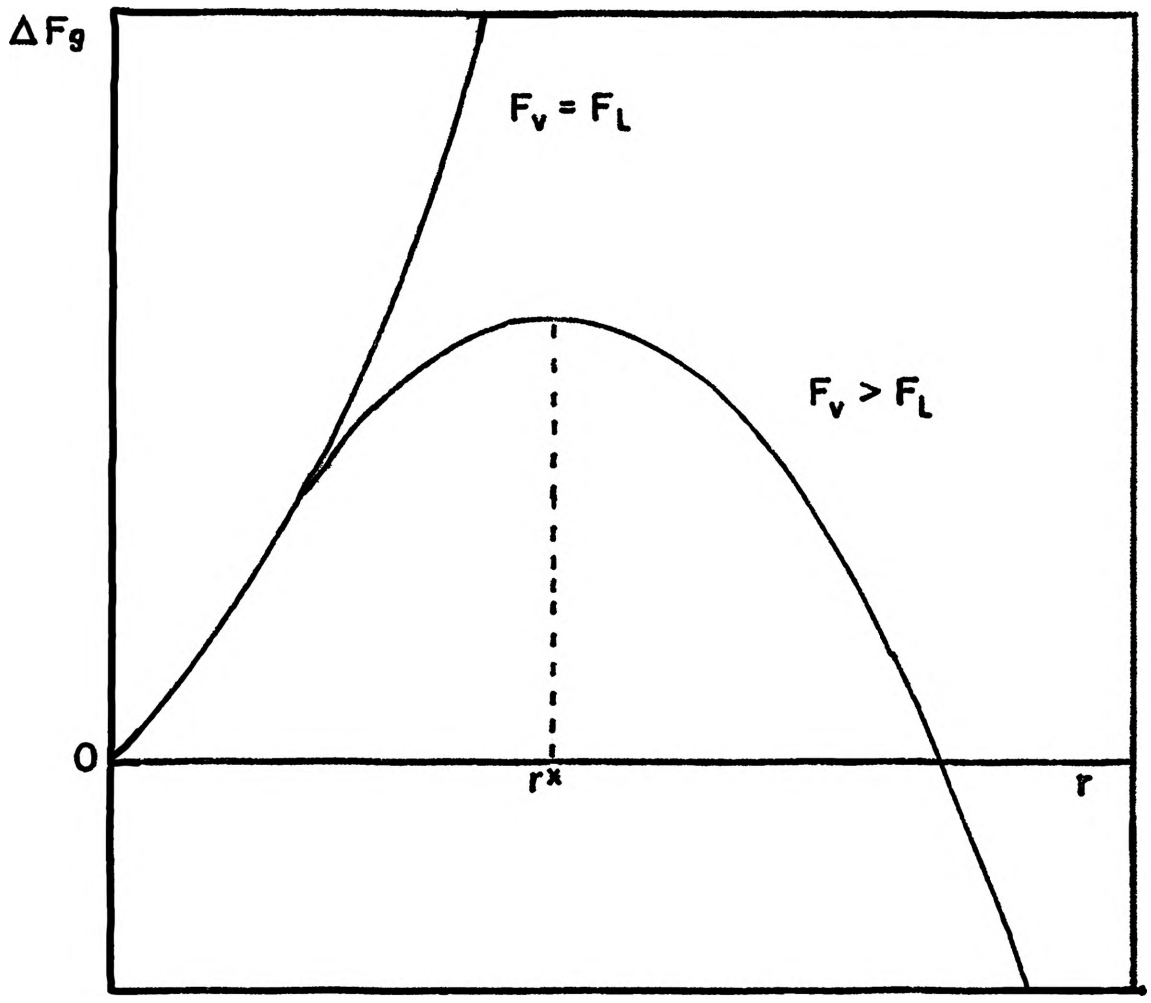

Figure 1

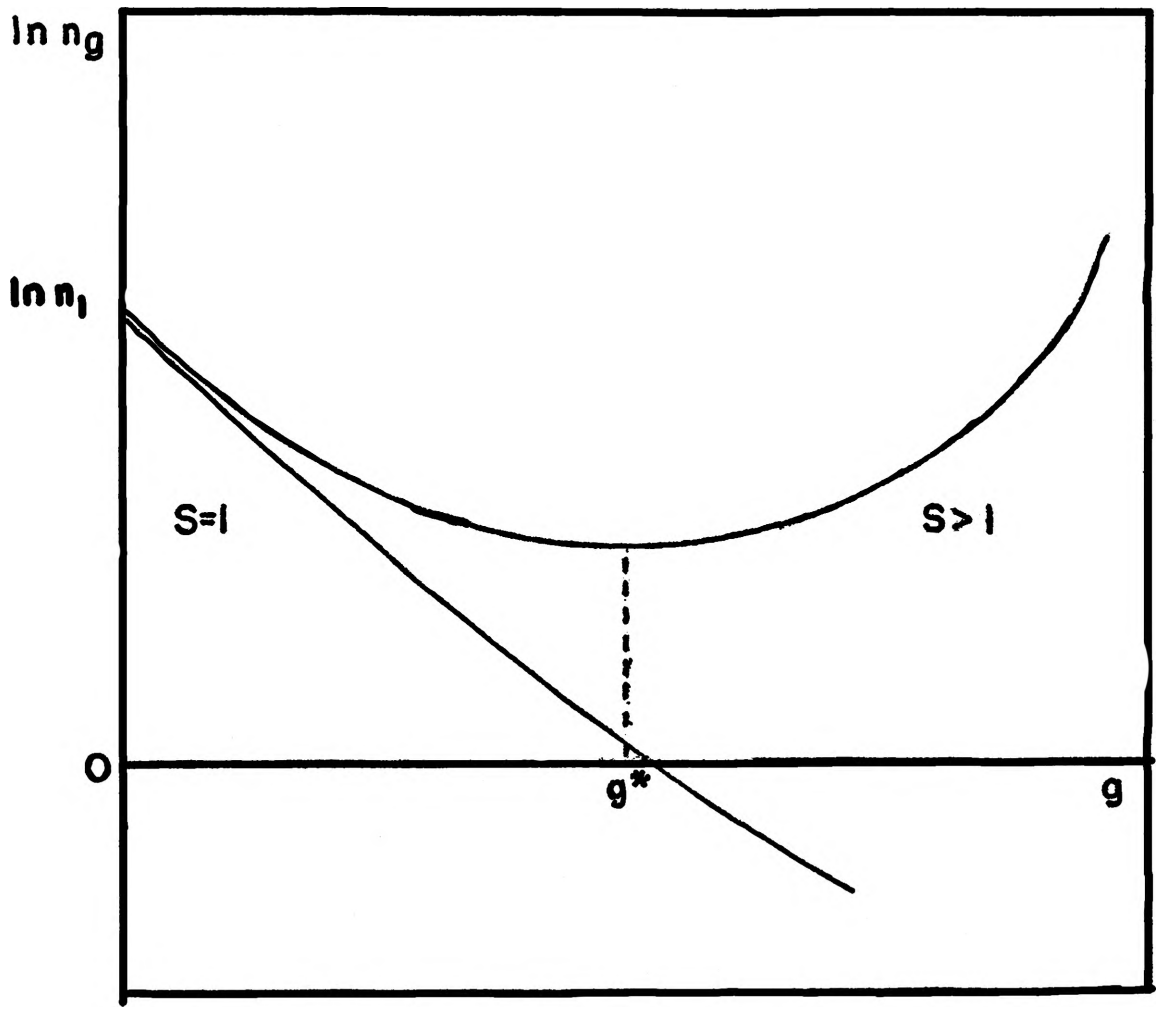

Figure 2

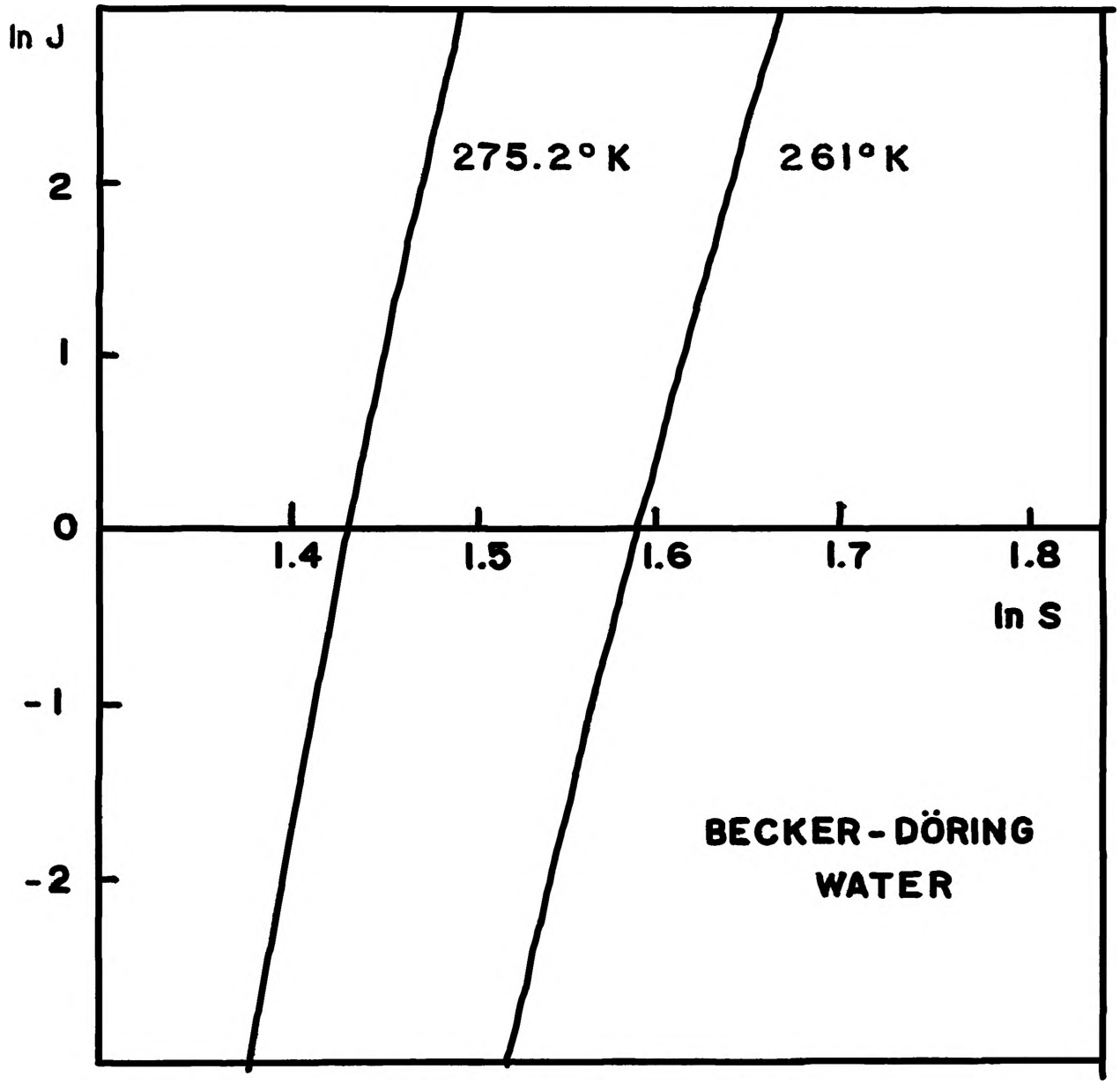

Figure 3

seemingly is essentially zero if S is below the critical level. Accordingly the liquid drop theories assume that once nuclei are formed and become free-growing, they are magically removed so as not to disturb the remaining system. No attempt is made in the classical theories to describe the rate of growth of the droplets once they have become free-growing or to account for depletion of the vapor. Classical nucleation theory only attempts to predict the rate at which free-growing droplets appear in the vapor.

3. Becker and Döring.[4] The nucleation rate theory of Becker and Döring is the classical calculation in the field of homogeneous vapor condensation and will be worked out in detail here. They consider the condensation process to involve a series of quasi-chemical reactions,

$$\begin{aligned} A + A &\rightleftarrows A_2 \\ A_2 + A &\rightleftarrows A_3 \\ &\cdots\cdots\cdots\cdots \\ A_{g^*} + A &\rightleftarrows A_{g^*+1} \\ &\cdots\cdots\cdots\cdots \\ A_{s-1} + A &\rightleftarrows A_s, \end{aligned} \tag{2-10}$$

with characteristic forward and reverse reaction rates. A represents a single vapor molecule and A_g represents a single g-mer. An idealized situation is considered in which clusters form, grow and then are removed from the system as soon as they reach a certain size, $g = s$, where $s > g^*$. This arbitrary cut-off has to be made or else the droplets, if allowed to grow indefinitely, would quickly outnumber the vapor molecules. This artifice also allows

the supersaturation to be considered essentially constant during nucleation. The number of droplets which reach the agreed size g = s per unit volume per second is called the nucleation rate. For computational purposes the vapor pressure is kept constant by the continuous introduction of single vapor molecules into the system.

A stationary distribution of cluster sizes is assumed to exist in the vapor. There will be a steady stream of clusters from one size to another moving through the distribution. The steady state is that condition which occurs when each of equations (2-10) has the same forward reaction rate. Courtney[2] has shown that such steady-state nucleation is obtained in expansion chambers within 0.5 μsec after the start of the expansion.

Becker and Döring assume that the nucleation process involves a sequence of slow reactions localized around cluster sizes near that of the nucleus, g*. Recalling the variation of ΔF_g with g, fig. 1, it is evident that this assumption amounts to saying that the nucleus is in metastable equilibrium with the supersaturated vapor. A small, but finite, disturbance of the nucleus, such as the addition or subtraction of a single molecule, is assumed to cause the nucleus either to become free-growing or to evaporate.

From the Boltzmann relation between entropy and probability, the probability for the appearance of a

nucleus in the supersaturated vapor is proportional to $\exp(-\sum/k)$, where $\sum$ is the total decrease in entropy in the formation of the nucleus at constant volume and constant internal energy. $\sum$, in turn, is given by[22]

$$\sum = A/T, \qquad (2\text{-}11)$$

where A is the work required to produce a nucleus isothermally and reversibly from g* vapor molecules at temperature T. Four separate processes contribute to A:

a. Removal of g* molecules from the vapor, $(-F_V g^*)$.

b. Isothermal expansion from the equilibrium pressure p* given by eq. (2-1) to the saturation vapor pressure, p_∞, at temperature T, $(-kT\ln p^*/p_\infty\, g^*)$.

c. Condensation of g* vapor molecules on a plane surface of the liquid, $(+F_V g^*)$.

d. Formation of the curved surface of the droplet, $(F^*\sigma)$, where F* is the surface area of a nucleus.

The sum of the work done in these four processes must equal A. The works done in processes a and c cancel each other exactly. Thus A is given by,

$$A = \sigma F^* - g^* kT \ln p^*/p_\infty, \qquad (2\text{-}12)$$

which is just eq. (1-6) written in terms of g* rather than r*. From the Kelvin eq., (2-1), we have

$$A = \sigma F^* (1 - g^*/F^*\, dF^*/dg^*), \qquad (2\text{-}13)$$

where dg* is the increase in the number of molecules in the nucleus for an increase dF* in surface area. Since

$$F^* = (\text{constant}) g^{*2/3},$$

we have,

$$g^*/F^* \, dF^*/dg^* = 2/3.$$

Hence,

$$A = 1/3 \, F^* \sigma \tag{2-14}$$

and from eq. (2-9), we have

$$J = K_2 \exp(-A/kT) = K_2 \exp(-\sigma F^*/3kT). \tag{2-15}$$

Becker and Döring evaluate K_2 kinetically using a method devised by Farkas.[21] The nucleation rate, J, is now thought of as a steady current through the distribution n_g $(1 \leq g \leq s)$. Let $\Lambda_g dt$ be the probability that from a cm^2 of the surface of a g-mer in time dt a molecule will evaporate; $\Gamma_o dt$ the corresponding probability that from the sensitive volume a molecule will condense on a surface area of 1 cm^2; and, finally, let $F_g' = n_g F_g$ be the total surface area of all the g-mers. Then for the current, J, we have

$$J = \Gamma_o F'_{g-1} - \Lambda_g F'_g, \quad 2 \leq g \leq s \tag{2-16}$$

which is nothing more than the detailed microscopic balance condition for dynamic equilibrium in the g-mer distribution. The probability for condensation, Γ_o, is considered to be proportional to the partial pressure, p*, of the vapor in the sensitive volume (which is the equilibrium vapor pressure of the nucleus). Similarly the probability for evaporation, Λ_g, is taken to be proportional to the vapor pressure of the g-mer, pg, which may be more or less than p* depending on whether the g-mer is smaller or larger in size than the nucleus. Defining $\beta_g = \Gamma_o/\Lambda_g$, we have the starting equation

$$F'_g = F'_{g-1}\beta_g - (J/\Gamma_o)\beta_g. \qquad (2\text{-}17)$$

For $g = g^*$ the equilibrium condition, $\beta_{g^*} = 1$, holds. For the other g-mers, we have the condition

$$\beta_g = p^*/p_g = \exp\left[2M\sigma/\rho RT(1/r^* - 1/r_g)\right]$$
$$= \exp\left[\alpha(1/r^* - 1/r_g)\right], \qquad (2\text{-}18)$$

which follows from Kelvin's equation and our collision-frequency growth assumption.

The formation and growth of the nucleus is represented by the equations ($s > g^*$),

$$\begin{aligned} F'_2 &= F'_1\beta_2 - (J/\Gamma_o)\beta_2 \\ F'_3 &= F'_2\beta_3 - (J/\Gamma_o)\beta_3 \\ &\cdots\cdots\cdots\cdots\cdots\cdots \\ F'_s &= F'_{s-1}\beta_s - (J/\Gamma_o)\beta_s. \end{aligned} \qquad (2\text{-}19)$$

For supersaturations of three or four, Table I shows that a rather large number of simultaneous equations can be involved in the calculation of J.

The total surface areas, F'_g, are first removed from equations (2-19) by dividing the first of these equations by β_2, the second by $\beta_2\beta_3$, etc, and finally the last by $\beta_2\beta_3\ldots\beta_s$. Adding the resulting equations, we have,

$$F'_s/(\beta_2\beta_3\ldots\beta_s) = F'_1 - (J/\Gamma_o)\left[1 + 1/\beta_2 + \ldots \right.$$
$$\left. \ldots + 1/(\beta_2\beta_3\ldots\beta_{s-1})\right]. \qquad (2\text{-}20)$$

As a result of this method of division, equations (2-19) have been put into the form ($i = 1, 2, \ldots s$)

$$\Phi_{i+1} = \Phi_i - JR_i, \qquad (2\text{-}19a)$$

where $$\Phi_i = F'_1/(\beta_2\beta_3\ldots\beta_i)$$

and $$R_i = 1/(\Gamma_o\beta_2\beta_3\ldots\beta_{i-1}).$$

Becker and Döring recognize eq. (2-19a) as a form of

Ohm's law with potential difference $\Phi_i - \Phi_{i+1}$, current J and resistance R_i. The nucleation process can then be considered as a series of resistances through which the nucleation rate J flows as a current between the potential difference $\Phi_1 - \Phi_s$. Equation (2-20) can then be written in the form

$$JR = J(R_1 + R_2 + \ldots + R_{s-1}) = \Phi_1 - \Phi_s = F_1', \tag{2-21}$$

since $\Phi_1 = F_1'$ and $\Phi_s = 0$. Also when evaporation predominates over the condensation, the condition,

$$\beta_g < 1, \qquad (1 \leq g < g^*) \tag{2-22}$$

holds. Similarly when condensation predominates over evaporation, we have the condition,

$$\beta_g > 1, \qquad (g^* < g \leq s) \tag{2-23}$$

R_i can then be written exactly as

$$R_i = 1/\Gamma_0 \exp\{\alpha[1/r_2 + 1/r_3 + \ldots + 1/r_i - (i-1)/r^*]\} \tag{2-24}$$

in view of eq. (2-18), where r_g is the radius of a g-mer and r* is the radius of the nucleus.

A new variable, x_g, is introduced,

$$x_g = r_g/r^* = (g/g^*)^{1/3} \tag{2-25}$$

from which follows the results $g = g^* x_g^3$ and $dg = 3g^* \ldots x_g^2 dx_g$. The sum in the exponential (2-24) can be replaced by the integral,

$$(1/r_2 + \ldots + 1/r_i) \simeq 1/r^* \int_{g=1}^{i} dg/x_g = 3g^*/r^* \int_{x_1}^{x_i} x_g dx_g = 3g^*/2r^*(x_i^2 - x_1^2). \tag{2-26}$$

From the above results, we have

$$1 = g^* x_1^3, \qquad i = g^* x_i^3, \tag{2-27}$$

and

$$i - 1 = g^*(x_i^3 - x_1^3). \tag{2-28}$$

Then eq. (2-24) can be written

$$\begin{aligned} R_i &= 1/\Gamma_o \exp\{\alpha[3g^*/2r^*(x_i^2 - x_1^2) \\ &\qquad - g^*/r^*(x_i^3 - x_1^3)]\} \\ &= 1/\Gamma_o \exp\{A'[(3x_i^2 - 2x_i^3) \\ &\qquad - (3x_1^2 - 2x_1^3)]\}, \end{aligned} \tag{2-29}$$

where $A' = \alpha g^*/2r^* = \sigma F^*/3kT$.

Figure 4 shows R_i vs x_i for water at 0°C with the assumptions $g^* = 100$ and $A = 10$. The significant feature of the curve is that the resistance, R_i, becomes greatest (at x_g^*) for the cluster size in the smallest concentration, namely the nucleus. Since reaction rates are proportional to reactant concentrations by the law of mass action, it must be the case that the reaction producing the nucleus has the smallest forward rate. Thus, in the steady state nucleation process envisioned by Becker and Döring in which all of the forward reaction rates are equal, the rate of nucleation is controlled by the forward rate of one reaction, namely

$$A_{g^*-1} + A \rightleftharpoons A_{g^*}. \tag{2-30}$$

Therefore, the nucleation rate depends ultimately on the concentration of the nucleus.

The next step is to replace the sum of resistances in eq. (2-21) by the integral

$$\int_1^s R_g\,dg = 3g^* \int_{x_1}^{x_s} Rx^2\,dx,$$

which can be rewritten in view of eq. (2-29) as

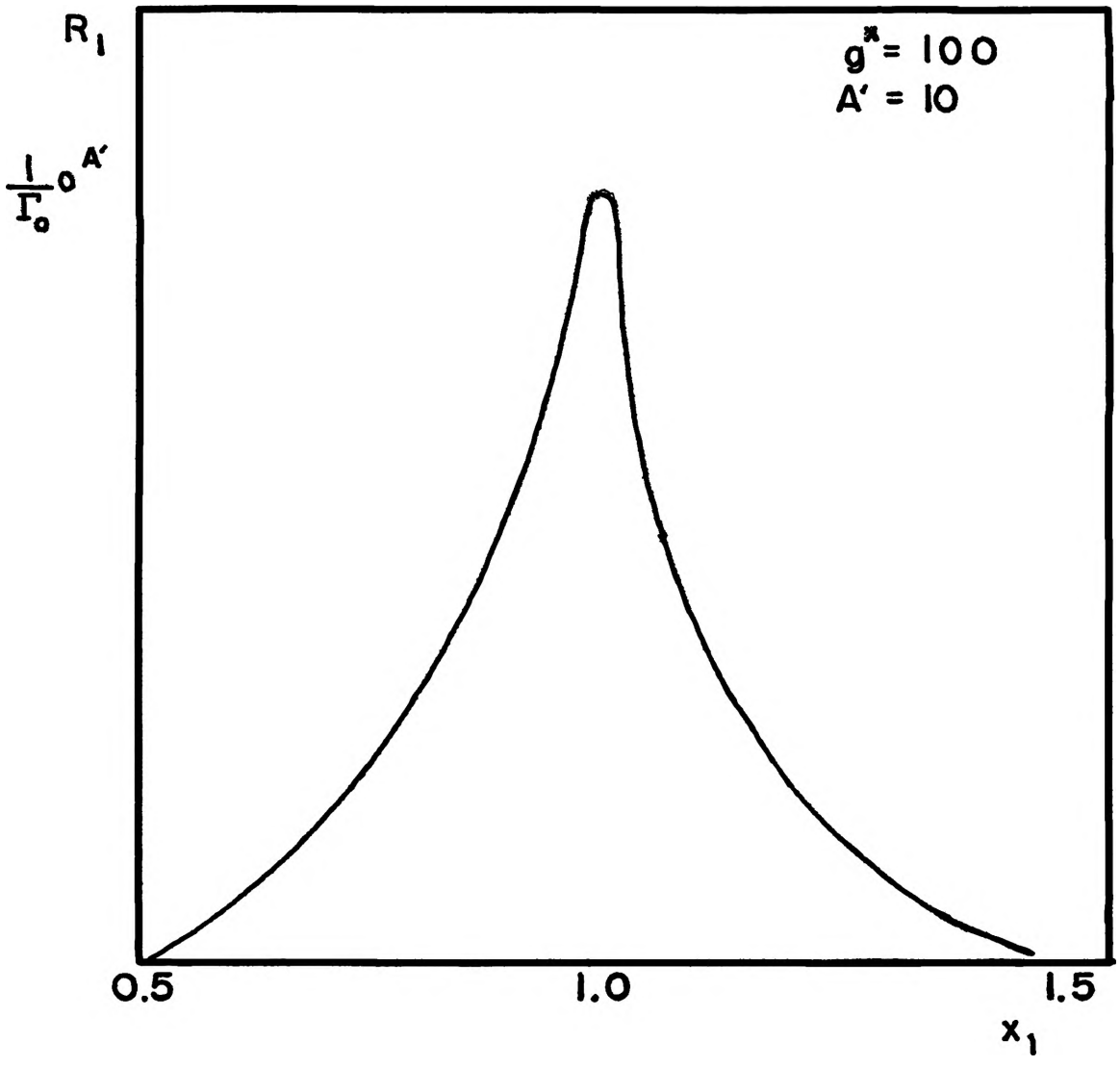

Figure 4

$$\int_1^s R_g dg = 3g^*/\Gamma_o \exp\left[-A'(3x_1^2 - 2x_1^3)\right] \int_{x_1}^{x_s} \exp\left[A'(3x^2 - 2x^3)\right] x^2 dx. \qquad (2\text{-}31)$$

For $x = 1$, that is, for the nucleus, Becker and Döring believe that the integrand of eq. (2-31) has a sharp maximum of magnitude $e^{A'}$ (cf. fig. 4). Setting $x = 1 + \xi$ and $3x^2 - 2x^3 = 1 - 3\xi^2 - 2\xi^3$, the integral in eq. (2-31) becomes

$$e^{A'} \int \exp\left[-A'(3\xi^2 + 2\xi^3)\right] (1 + \xi)^2 d\xi. \qquad (2\text{-}32)$$

Since A' ranges from 20-50 for water near room temperature when $10 < g^* < 100$, the integrand in eq. (2-32) is sharply peaked at $\xi = 0$ and, hence, that integral can be approximated by

$$\int_{-\infty}^{\infty} \exp(-3A'\xi^2) d\xi. \qquad (2\text{-}33)$$

Finally, if $3x_1^2 - 2x_1^3$ is neglected with respect to unity, then we have,

$$R = \int_1^s R_g dg = 3g^*/\Gamma_o \, (\pi/3A')^{1/2} \, e^{A'}. \qquad (2\text{-}34)$$

The nucleation rate then follows from eqs. (2-21) and (2-34),

$$J = \Gamma_o F_1'/g^* \, (A'/3\pi)^{1/2} e^{-A'}, \qquad (2\text{-}35)$$

where F_1' has been substituted for F_g'. The factor $\Gamma_o F_1'$ is twice the total number of collisions among the vapor molecules. From the kinetic theory of gases, we have

$$\Gamma_o F_1' = n_1 \bar{v}/\lambda, \qquad (2\text{-}36)$$

where n_1 = the vapor molecule concentration,

$\bar{v}$ = the mean molecular speed,

λ = the mean free path.

Since λ is inversely proportional to n_1, we may write

$$\Gamma_o F_1 = n_1^2 \bar{v}/\lambda_o N_o$$
$$= N_o (8/\pi R)^{1/2} T_o/p_o \lambda_o \qquad (2\text{-}37)$$
$$M^{-1/2} p^2/T^{3/2},$$

where the subscript $_o$ refers to values at standard conditions and N_o is Avogadro's number. A graph of eq. (2-37) is shown in fig. 5, curve A.

Several objections can be raised to the Becker-Döring theory. First, the assumption concerning A in eq. (2-32) is not justified since the surface tension, σ, is not known for small droplets of water. In fact, Courtney[2] shows that the integrand of eq. (2-31) has a broad rather than a sharp maximum at $g = g^*$. This means that the concentration not only of the nucleus, but also that of cluster sizes near the size of the nucleus must control the nucleation kinetics. Secondly, in eq. (2-35) the total surface area of the vapor molecules, F_1', replaces the total surface area of the g-mers, F_g', an assumption which cannot really be physically justified in this case.

There is, in addition, some question as to the appropriateness of considering embryos of twenty molecules or so as well-defined liquid droplets possessing the thermodynamic properties of the bulk liquid. The boundary layer separating the liquid and the vapor phases is not a unique geometrical surface but, rather, is a transition layer in which the properties of the vapor pass over to those of the liquid in a distance of a few molecular

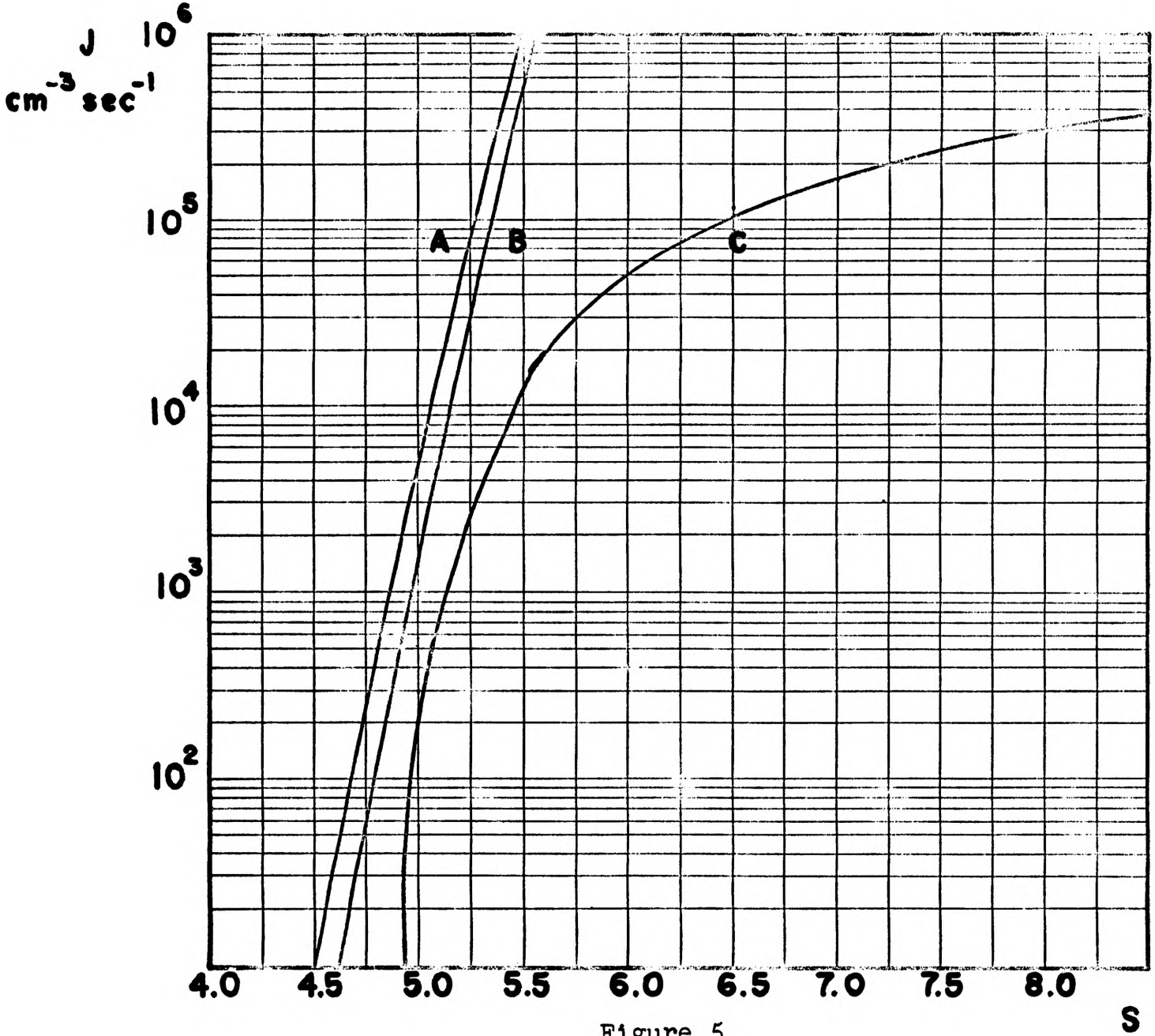

Figure 5

diameters,[5,25] For a small embryo the thickness of this transition layer is of the same order of magnitude as the radius of the nucleus. Hence, the radius, r*, is ambiguous. In view of these difficulties the Becker-Döring theory can be expected only to yield an order of magnitude estimation for the nucleation rate.

4. Frenkel.[5] This author utilizes the Becker-Döring assumptions, but converts the difference equations (2-19) into differential equations with g as the independent variable. He assumes that the integrand in eq. (2-31) has a sharp peak at $g=g^*$, but uses F'_{g^*} in place of F'_g. The Frenkel nucleation rate is given by the equation (cf. fig. 5, curve B)

$$J = n_1^2 (2m\sigma/\pi)^{1/2} \, 1/\rho \exp\left[(-16\pi\sigma^3 m^2)/3\rho^2 (kT)^3 (\ln S)^2\right]. \qquad (2\text{-}38)$$

5. Courtney.[2] This author is one of the more recent and prolific writers on the subject of vapor condensation. His investigation of non-steady state nucleation indicates that the steady-state nucleation is reached within 0.1 μsec after an infinitely fast expansion to a given level of supersaturation. An expansion chamber is much too slow a device to do anything with non-steady state nucleation.

Courtney has developed a steady-state theory of nucleation and growth. He permits the nucleation rate to vary during condensation, a much more realistic model of the condensation process. The corrected Frenkel nucleation rate,

$$J = n_1^2/S\ (2m\sigma/\pi)^{1/2}\ 1/\rho$$
$$\exp\left[(-16\pi\sigma^3 m^2/\ 3\rho^2(kT)^3(\ln S)^2\right], \quad (2\text{-}39)$$

is used to describe the nucleation process. A simple collision-frequency growth law,

$$k_g = uF_g = (kT/2\pi m)^{1/2} a g^{2/3}, \quad (2\text{-}40)$$

where k_g is the forward rate constant for the reaction

$$A_g + A \rightleftharpoons A_{g+1},$$

a is the mole fraction of vapor in the system, m is the mass of a single water molecule and u is the specific collision frequency, is assumed by Courtney to govern the growth of the nuclei. He neglects the evolution of heat by the growing droplets and assumes that the vapor distribution remains uniform, i.e. he neglects vapor diffusion as a regulatory mechanism in the droplet growth process. The computational procedure is as follows: An initial supersaturation ΔSS, is selected. A nucleation rate, $\mathcal{I}$, is calculated for that S from eq. (2-39). This rate is assumed to persist for an arbitrary time interval $\tau = 0.002$ sec. The total number, N, of nuclei produced in time τ is given by

$$N = \int_0^{\tau} J dt = \bar{J}\tau, \quad (2\text{-}41)$$

where $\bar{J}$ is an appropriate average nucleation rate during the time τ. The change in concentration of the vapor, Δn_1, due to the growth of the N nuclei is calculated using eq. (2-40). From eq. (1-1) a new and invariably lower supersaturation is calculated and the process is repeated for the next time interval using this new S.

From these computations the variation of the total number of condensing droplets, N_{total}, with time for a given initial S can be obtained (cf. fig. 6). In figure 7 the average nucleation rate is plotted as a function of the initial supersaturations with the sensitive time as the parameter. A modified form of Courtney's computation which takes into account the warming effects of the condensing vapor molecules is presently being attempted by a member of this research group.

Experiment

Measurements of homogeneous nucleation rates are almost non-existent in the literature. Most experimental endeavors in the field of vapor condensation have been of the critical supersaturation variety. Kassner and Allard[12] have attempted to bring the critical supersaturation measurements of Madonna, et. al.,[19] Volmer and Flood,[20] Sander and Damköhler,[26] and Powell[14] into agreement with their homogeneous nucleation rate measurements. Differences in chamber design and observational technique among these researchers cause considerable difficulty in intercomparing their results.

6. Frey.[11] Of all the researches done in the field of vapor condensation, those of Frey are most similar to what is done here. His chamber (volume 18 cm^3) is quite a bit smaller than ours (volume 3000 cm^3) and has a sensitive time of 0.1 sec. Observation of droplet concentrations is done photographically. His results are

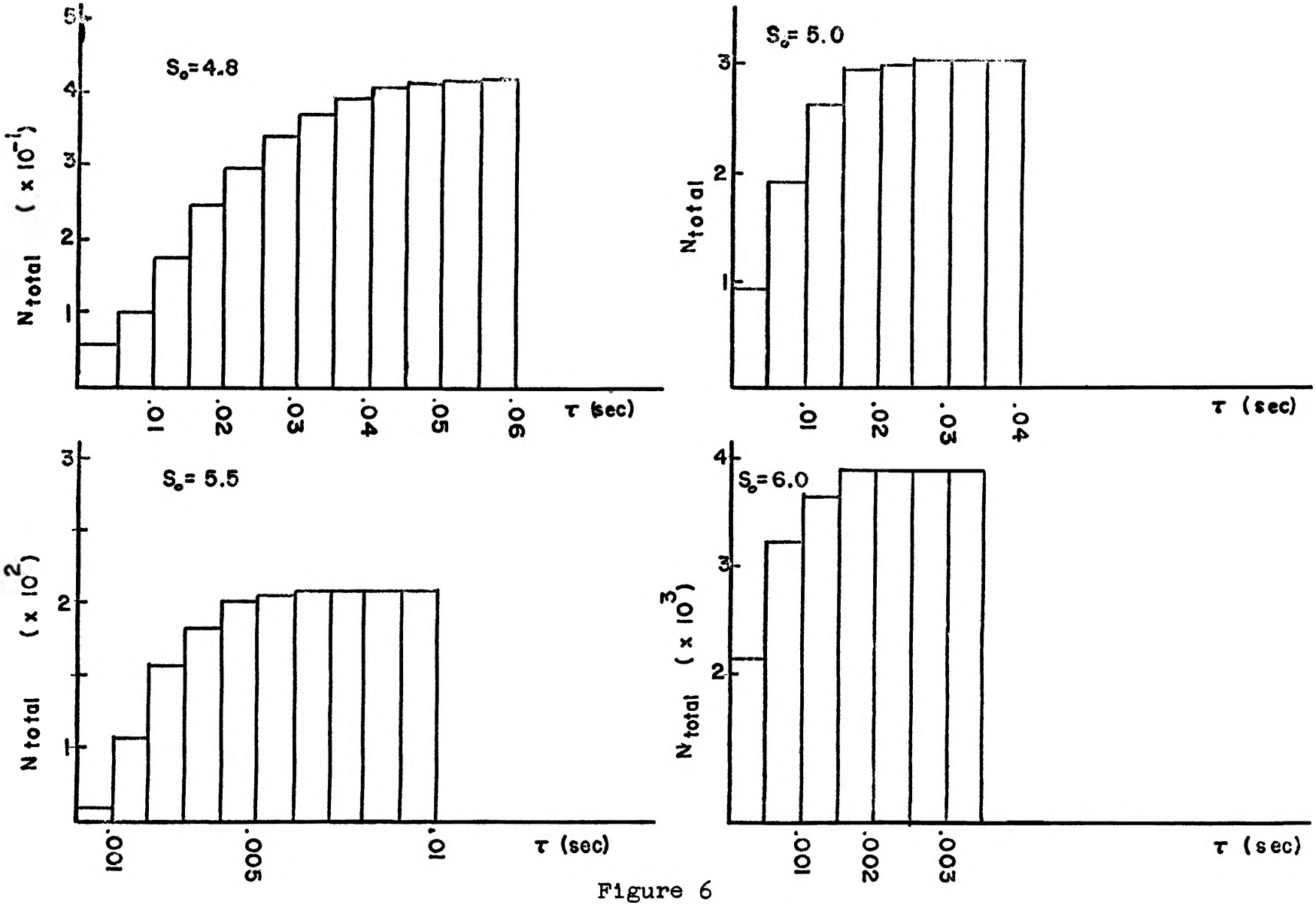
S_o= 4.8
N_{total} (x 10^{-1})
.01
.02
.03
.04
.05
.06
τ (sec)
S_o= 5.0
N_{total}
.01
.02
.03
.04
τ (sec)
S_o= 5.5
N total (x 10^{2})
.001
.005
.01
τ (sec)
S_o= 6.0
N_{total} (x 10^{3})
.001
.002
.003
τ (sec)

Figure 6

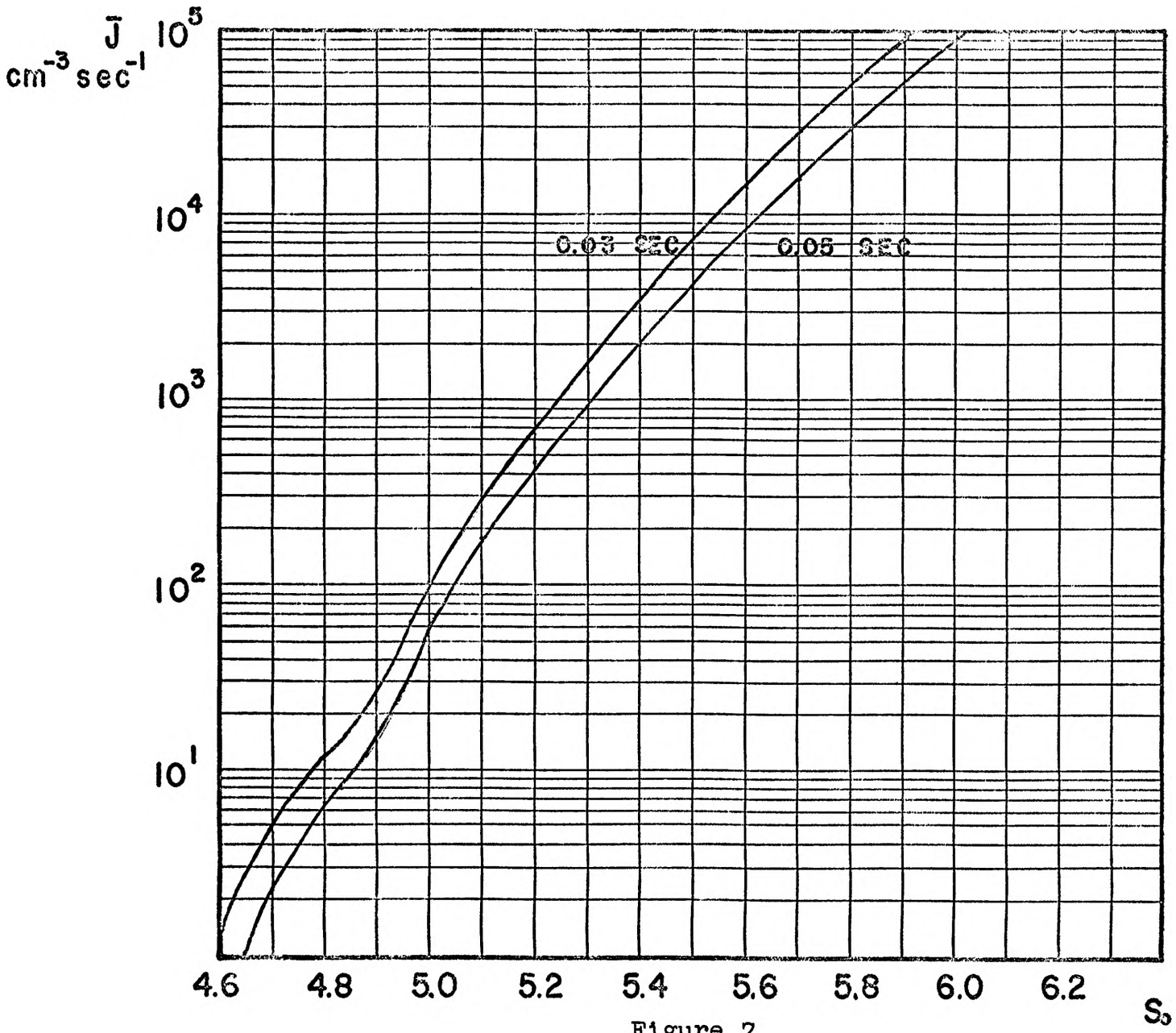
$\bar{J}$
$cm^{-3}\,sec^{-1}$
10^5
10^4
10^3
10^2
10^1
0.03 SEC
0.05 SEC
4.6
4.8
5.0
5.2
5.4
5.6
5.8
6.0
6.2
S_s

Figure 7

given in fig. 5, curve C. Mason[3] has discussed the pronounced flattening of the J vs. S curve for $S > 6.0$ and concludes that vapor depletion and heating effects are combining to lower the observed nucleation rates. Extrapolation of Frey's curve shows that his fog limit (~ 1 droplet/cm^3) occurs at $S = 4.9$. The supersaturations reported by Frey must, however, be ambiguous since S is steadily and rapidly decreasing during the sensitive time of his chamber due to vapor depletion and heating effects. A clear-cut comparison between theory and experiment cannot truly be made when the condensation process occurs over a wide range of supersaturations and nucleation rates unless these variations in J and S are taken into account. In the following chapters a technique for overcoming such difficulties and arriving at an empirical relation between J and S will be discussed.

CHAPTER III

EXPANSION CHAMBER CHARACTERISTICS AND TECHNIQUES

The object of the experiments performed by this author is to obtain a clear-cut empirical relation between nucleation rate and supersaturation in the condensation of water droplets from a water vapor-helium mixture. This work is an extension of the work begun in August, 1963 by Allard, who obtained some preliminary data on nucleation rates. Since that time this writer has been engaged in solving some of the technical problems which plagued previous measurements. In this chapter brief descriptions of the expansion chamber and associated techniques of measurement will be given. For a more thorough discussion of the design of the chamber, the reader is referred to Allard's thesis.

1. Chamber Cycle. Figure 8 shows the essentials of our expansion chamber. It is a Blackett-type chamber with an outside diameter of 14 inches. The chamber is pressure-defined, which means that the initial position of the piston is determined by the pressure in the lower chamber. The magnitude of the expansion is determined by the "on" time of a valve and not by a stop. Hence, the piston need not seat at the end of the main expansion.

This chamber design has several advantages over a

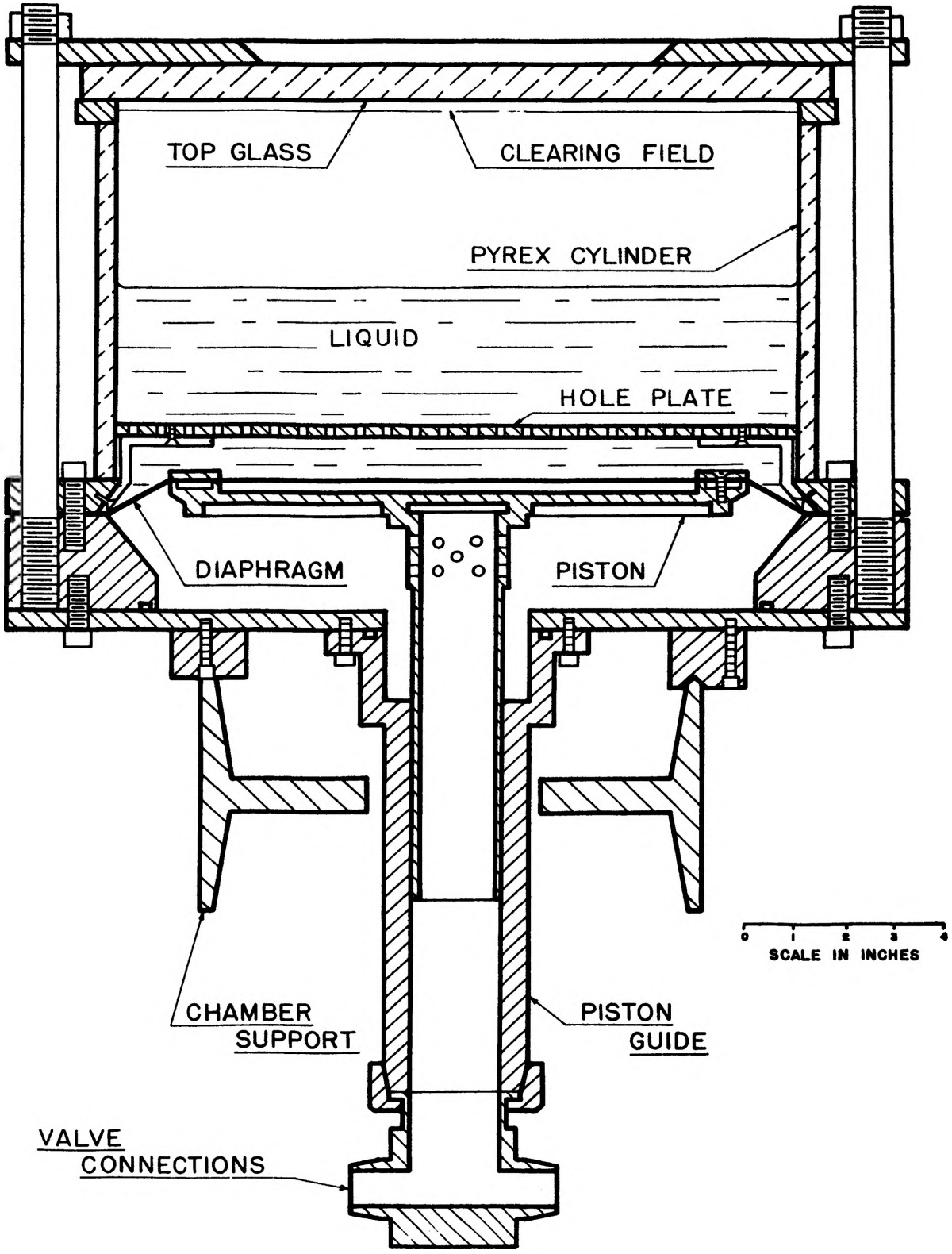
TOP GLASS
CLEARING FIELD
PYREX CYLINDER
LIQUID
HOLE PLATE
DIAPHRAGM
PISTON
0 1 2 3 4
SCALE IN INCHES
CHAMBER SUPPORT
PISTON GUIDE
VALVE CONNECTIONS

Figure 8

volume-defined chamber, i.e. one in which stops determine the magnitude of the expansion. These advantages can be elucidated by considering a typical chamber cycle diagrammed in fig. 9. The curve is somewhat idealized since oscillations occur at several places (cf. fig. 15). A large, rapid expansion, AB, establishes a desired initial supersaturation by producing a cooling effect in the vapor. A large thermal gradient exists during and after this expansion between the glass chamber walls and the gas-vapor mixture. The temperature of the sensitive volume begins to rise immediately upon the termination of the expansion at B due to compressive heating effects and droplet growth, thus quickly lowering the initial supersaturation level. Figure 10 shows chamber isotherms as a function of time after the main expansion. The calculation of these isotherms is based on a simplified model of the heat conduction process and is thoroughly worked out in Allard's thesis.

If S is greater than the ion limit at B, condensation will be observed on the tracks of ionizing particles during the time BC. It is desirable to maintain the value of S established at B as nearly constant as possible in the center of the chamber during BC in order that the droplets can grow quickly to photographable size. A slow, continuing expansion during BC offsets the rise in in temperature of the center of the sensitive volume from compressive heating and enables one to maintain a

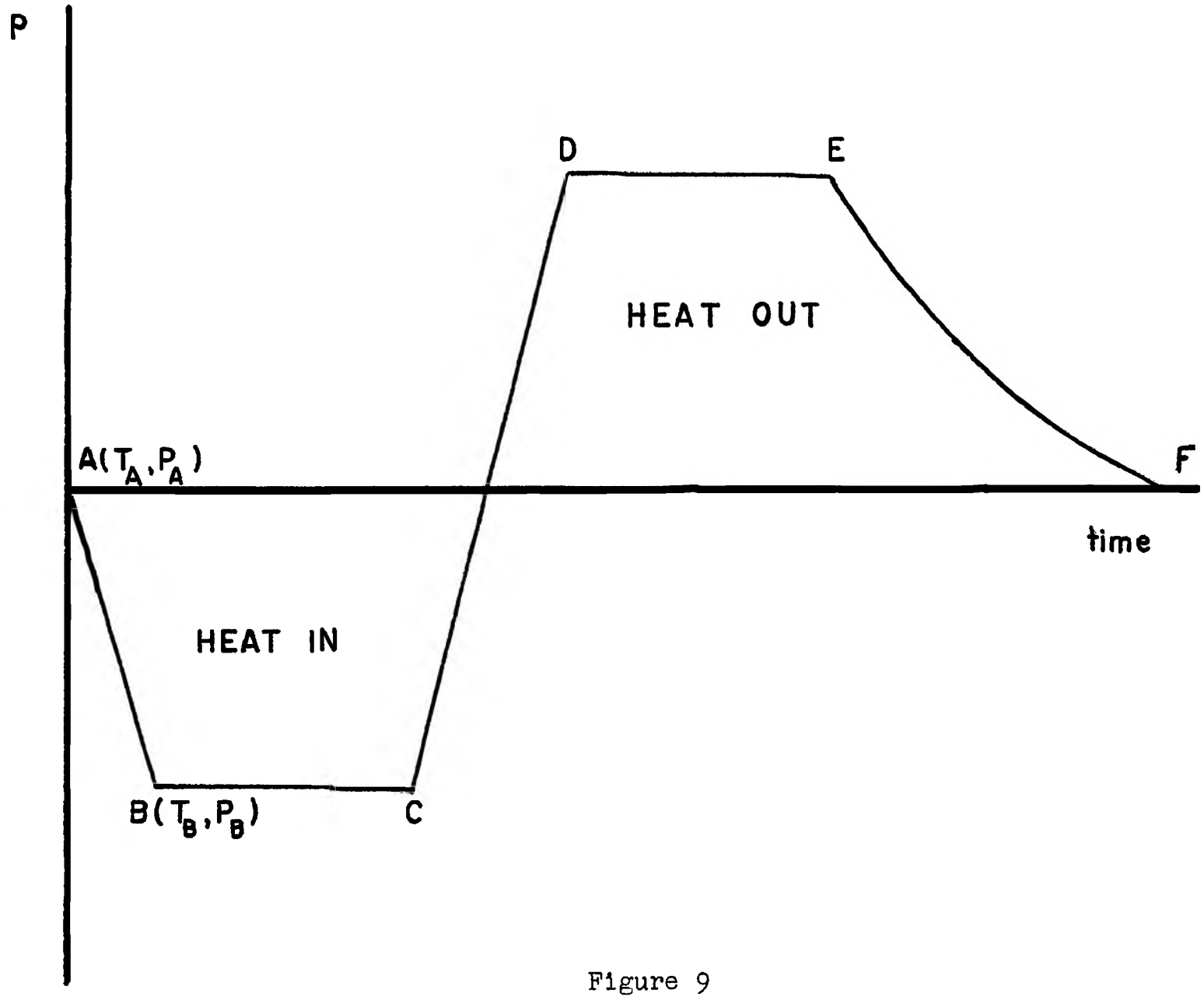

Figure 9

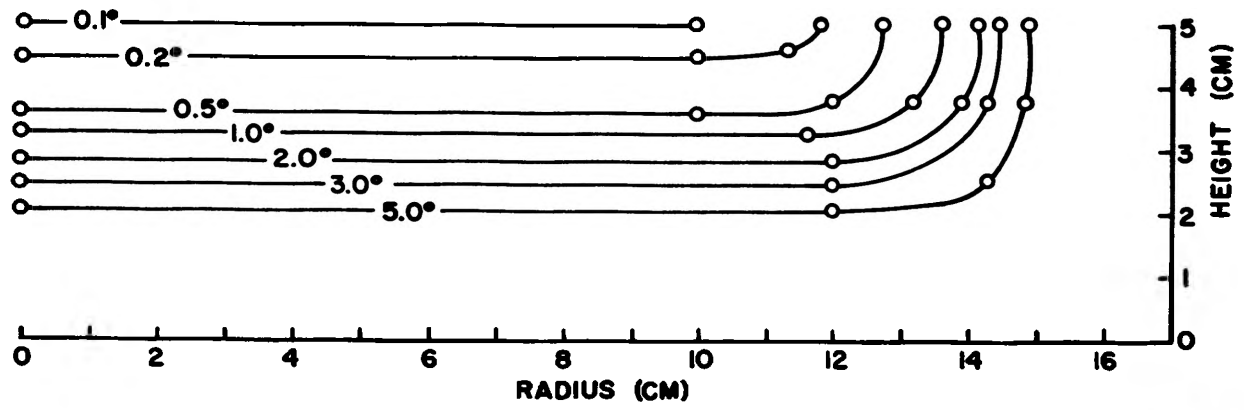

1.0 SEC. AFTER EXPANSION

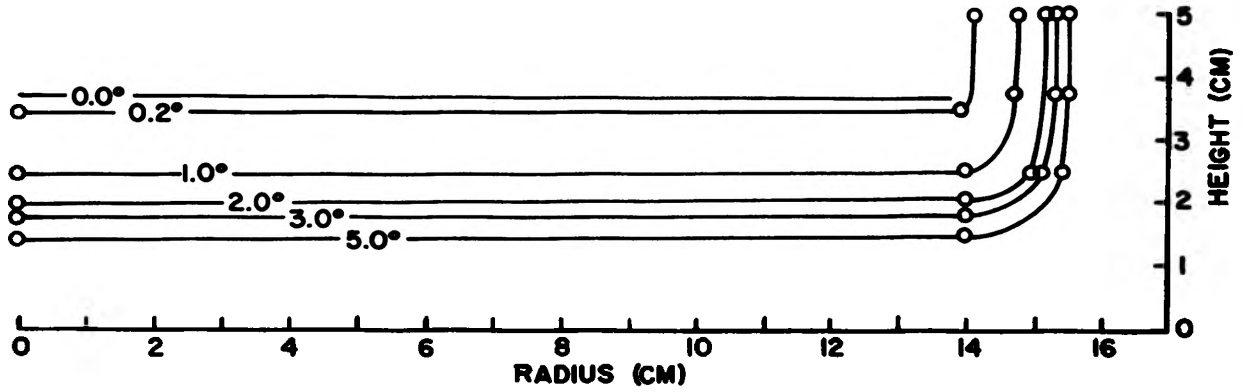

0.5 SEC. AFTER EXPANSION

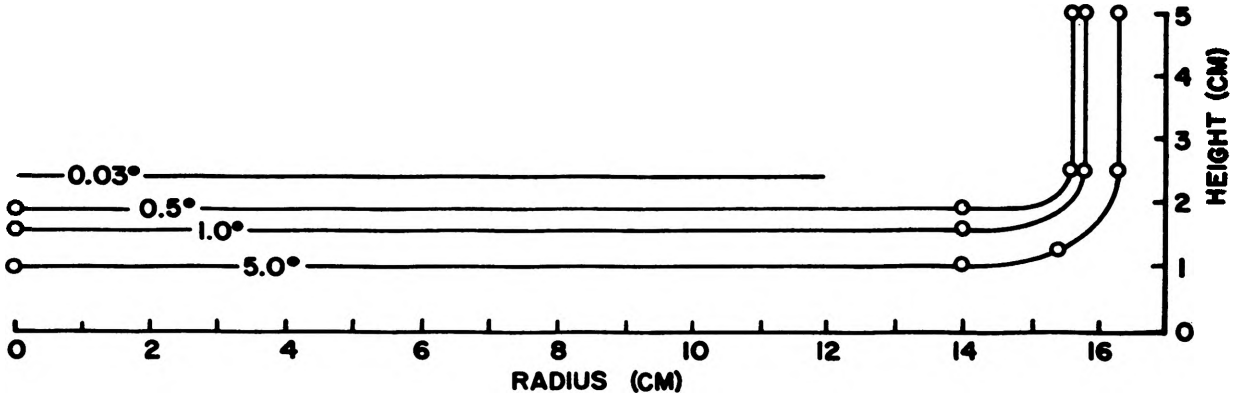

0.25 SEC. AFTER EXPANSION

Figure 10

constant supersaturation for about one second. This is ample time for making all necessary measurements. In these experiments the sensitive time is usually 0.03 sec. The pressure-defined chamber allows such an expansion whereas with a volume-defined chamber it would be impossible.

Having formed a number of droplets, it is next desirable to remove them completely from the chamber and so restore the sensitive volume to its initial conditions at A. To this effect a large compression, CD, is next made which causes the temperature of the sensitive volume during time DE to rise 20-30 C° above the initial temperature, T_A, at A. Heat flows out of the chamber rapidly and the object is to hold the chamber in this compressed state until all of the heat which flowed into the chamber during time AC can flow out during time DE. Thus one strives for a balance between "heat in" and "heat out" with the goal of returning the chamber to the initial conditions at A. The reader is referred to Packwood's thesis in which this problem is discussed in detail.[27]

During time DE the droplets rapidly evaporate under the sub-saturated conditions produced by the over-compression and leave behind in the sensitive volume sub-microscopic, thermodynamically stable residues called "re-evaporation nuclei."[10] These re-evaporation nuclei are much larger than the critical size required by Kelvin's equation for equilibrium with the vapor and, hence, will

act as super-size condensation centers on subsequent expansions if they are not removed from the sensitive volume in some way. Therefore, a show expansion, EF, is next performed in which a slight supersaturation is obtained. Because of their large size the re-evaporation nuclei condense vapor easily for $S \simeq 2$ and, hopefully, will grow so large during EF that their weight will cause them to fall into the liquid. Allard[10] has made qualitative studies which indicate that this method is effective for removing all of the re-evaporation nuclei.

The entire cycle from A to F takes approximately 40-50 seconds. A four minute waiting interval follows F during which the sensitive volume becomes saturated at the initial temperature, T_A. Measurements made by Packwood[27] show that this length of time is adequate to allow the sensitive volume to equilibrate.

2. Gas-Vapor Mixture. Several gallons of demineralized, distilled water are placed in the chamber and dyed black to produce a photographable background. The temperature of the liquid is monitored with a chromel-alumel thermocouple and can be regulated by means of a thermostating device. The liquid temperature is usually about 18-23 ^{o}C and is regulated to ± 0.05 C^{o}. At these temperatures the vapor pressure of water is approximately 20 mm. Hg. The air and the dissolved gases which evaporate from the liquid are flushed out with helium prior to each series of experiments so that a helium-water

vapor mixture remains. With the piston in the fully expanded position, the pressure of the mixture is about 1.3 atmospheres absolute. Compressed air is allowed to raise the piston to its ready position at which the pressure of the mixture is about 2.0 atmospheres absolute.

The presence of the helium has desirable effects on the condensation process. The thermal conductivity of helium helps conduct heat away from the growing droplets and thus helps maintain a high supersaturation in the nearby vapor. In addition, the helium provides a convenient adiabatic index ($\gamma = 1.6600$)[24] the importance of which will be discussed below. Finally, the pressure of the helium, which accounts for most of the pressure in the chamber, provides a driving force which increases the speed of the falling piston.

Such rapid expansions will cause convection currents to arise in the chamber. Near the center of the chamber convection is predominantly in the direction of the falling piston. Droplets in this region fall vertically toward the surface of the liquid. It is assumed that the droplet motion will not alter droplet concentrations one would observe if no motion occurred.

A small temperature difference of approximately 0.5 C^{o} is maintained between the top glass and the liquid with the former at the higher temperature. Condensation on the top glass, which obscures the sensitive volume,

is thus eliminated. The thermal gradient established in the sensitive volume by this temperature difference also helps stabilize the sensitive volume during the waiting interval so that no convection currents are present immediately before the expansion. Thermocouple measurements made on the quiescent chamber indicate that the thermal gradient is constant from top to bottom near the center of the chamber. Thermocouples on the top glass and in the liquid enable one to control the gradient to within $\pm$ 0.01 C^{o}. The reference junctions of the thermocouples are inserted in a thermostated Dewar containing water which is maintained at 23,50 $\pm$ 0.01 ^{o}C. The thermocouples are monitored with a Keithley Milli-Microvoltmeter.

3. Valving. The position of the piston is controlled pneumatically by means of a system of valves shown schematically in fig. 11. Figure 12 shows a specially constructed solenoid expansion valve used to produce the main expansion. The chamber is connected to a vacuum tank through this valve in order to increase the pressure differential between the chamber and the room during an expansion. A fast expansion (0.11 sec. to the fog limit) results. The chamber is connected to fifteen separate valves which allow an almost limitless variety of expansions and compressions to be intermixed in a single duty cycle. The magnitude of an expansion or compression is determined by the size of the valve

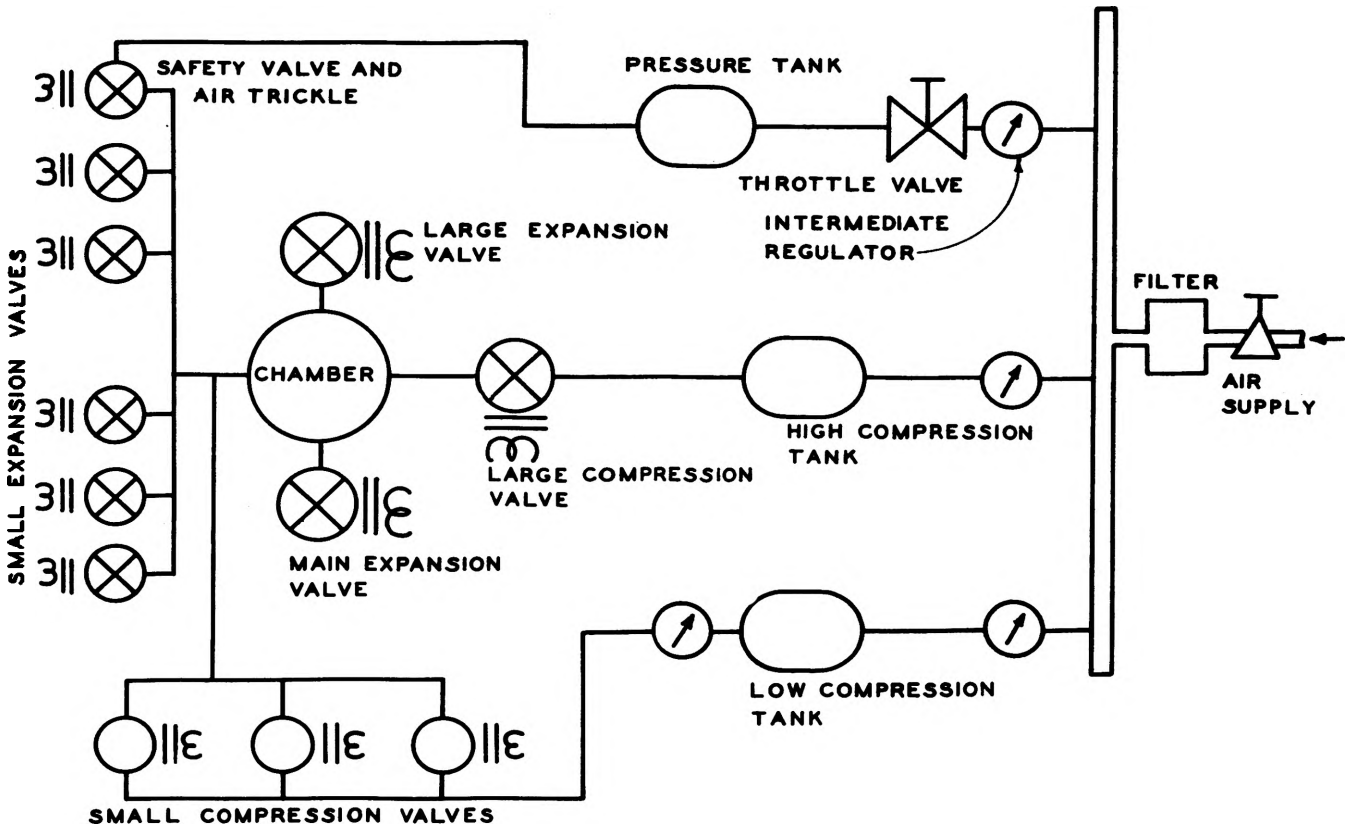
SAFETY VALVE AND
AIR TRICKLE
PRESSURE TANK
THROTTLE VALVE
INTERMEDIATE
REGULATOR
FILTER
AIR
SUPPLY
LARGE EXPANSION
VALVE
SMALL EXPANSION VALVES
CHAMBER
LARGE COMPRESSION
VALVE
HIGH COMPRESSION
TANK
MAIN EXPANSION
VALVE
LOW COMPRESSION
TANK
SMALL COMPRESSION VALVES

Figure 11

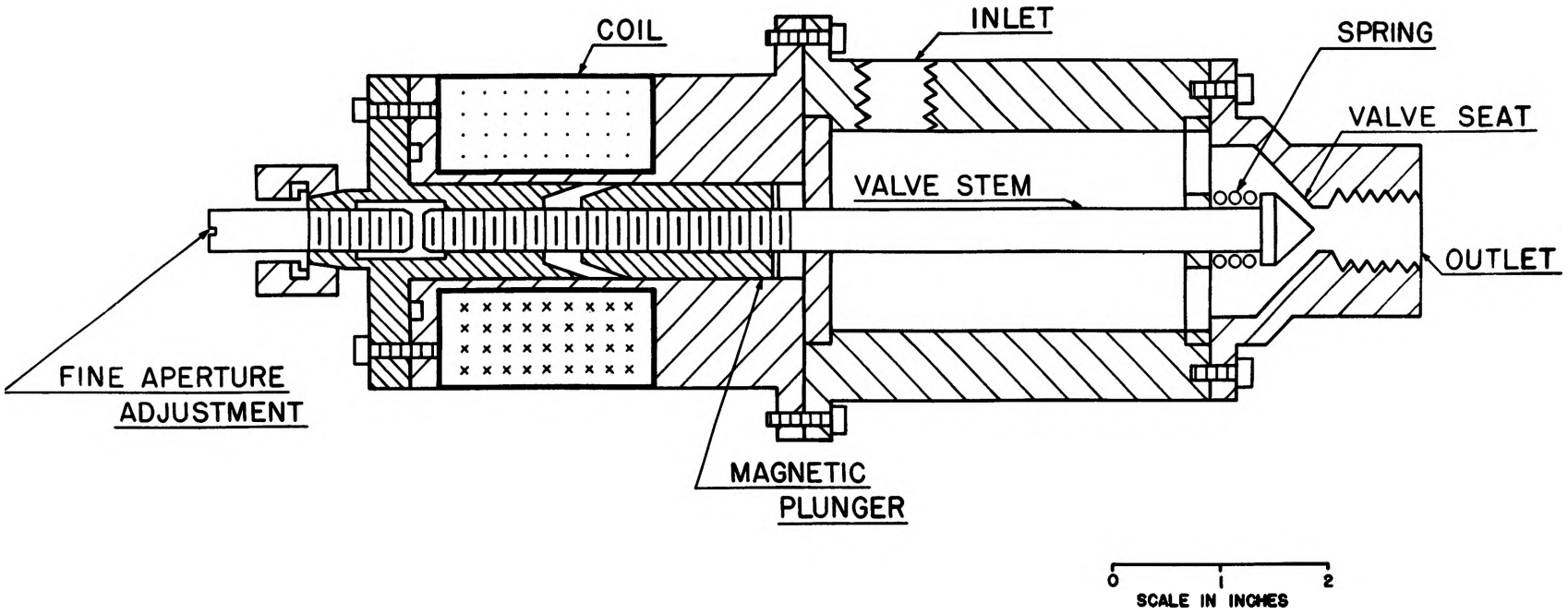
COIL
INLET
SPRING
VALVE SEAT
VALVE STEM
OUTLET
FINE APERTURE
ADJUSTMENT
MAGNETIC
PLUNGER
0
1
2
SCALE IN INCHES

Figure 12

orifice and the time that the valve is open, both of which can be finely adjusted. The successful programming of a duty cycle depends largely on the skill and experience of the operator. A considerable length of time is required to learn the necessary technology.

4. Valve Timing. Valve timing is completely electronic. The master timer and a single valve timer are shown in figures 13 and 14 respectively. The master timer initiates the cycle with a master pulse, resets the individual function timers during the waiting interval and determines the duration of the recovery period between expansions. All of the timing circuits are built up from a basic thyratron circuit which has the merits of simplicity and reliability. The master pulse at time t will activate the "start" thyratron of a valve timer at time t_1 and the valve will open. At time t_2 ($t \leq t_1 \leq t_2$) the "stop" thyratron will fire and close the valve. Times t, t_1 and t_2 are determined by the time constant of an RC circuit in each thyratron grid circuit. The timers are accurate to $\pm$ 0.001 sec. Mechanical and electrical time constants in the solenoid valves cause an estimated delay in response of about 0.02 sec. Reproducibility, however, is not affected severely by such delays. A cycle is programmed simply by adjusting the time constants of the RC circuits by means of potentiometers.

The relays employed in the timing circuits are

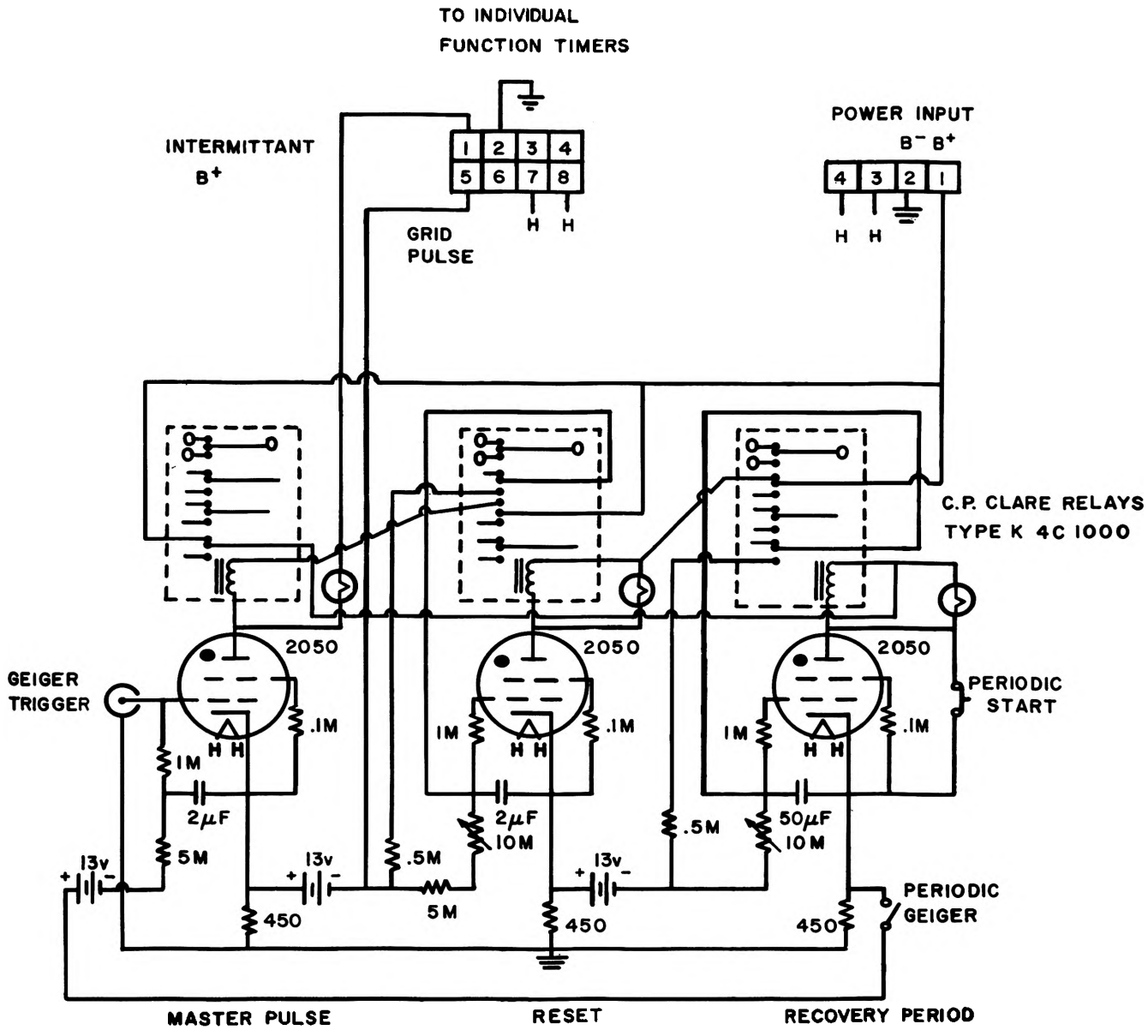
TO INDIVIDUAL
FUNCTION TIMERS
INTERMITTANT
B+
GRID
PULSE
1 2 3 4
5 6 7 8
H H
POWER INPUT
B- B+
4 3 2 1
H H
C.P. CLARE RELAYS
TYPE K 4C 1000
2050
2050
2050
GEIGER
TRIGGER
PERIODIC
START
.1M
1M
2μF
5M
13v
450
.5M
10M
50μF
PERIODIC
GEIGER
MASTER PULSE
RESET
RECOVERY PERIOD

Figure 13

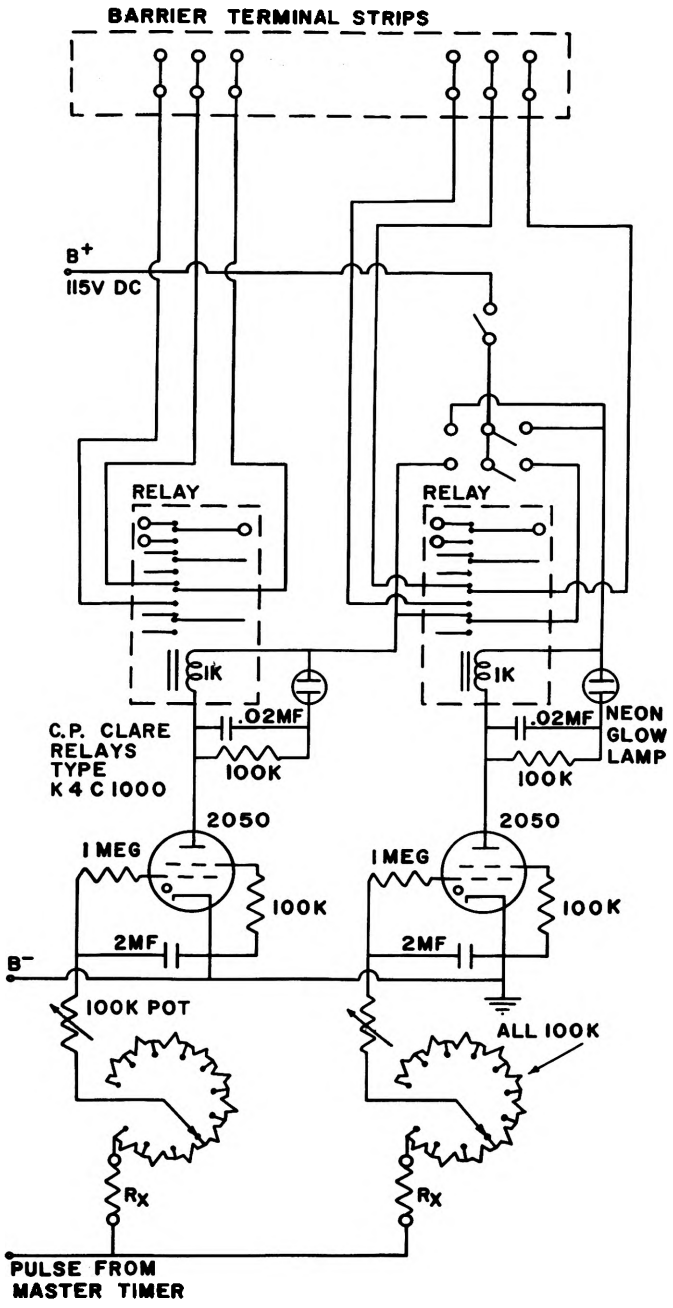
BARRIER TERMINAL STRIPS
B+
115V DC
RELAY
RELAY
1K
1K
.02MF
.02MF
NEON
GLOW
LAMP
C.P. CLARE
RELAYS
TYPE
K 4 C 1000
100K
100K
2050
2050
1 MEG
1 MEG
100K
100K
2MF
2MF
B-
100K POT
ALL 100K
Rx
Rx
PULSE FROM
MASTER TIMER

Figure 14

quite small. These are used because they possess very fast response times which are quite reproducible. In order to use the small contacts on the heavy d.c. loads required by the special solenoid valves, the relay contacts must be protected by a properly chosen resistor-capacitor arrangement. These have been found to give better protection than the semiconductor devices currently on the market. For the large valves two sets of contacts are placed in series to increase the rate at which the contacts open. A 10 μfd capacitor with a 600 volt rating is paralleled with a 10,000 ohm, 1 watt resistor and placed across the contact. This arrangement provides adequate protection for the small relays which handle up to 6 amps at 90 vdc going to the solenoid valves.

5. Signal Conditioning Systems. Provision has been made to measure the pressure, volume and temperature of the sensitive volume. The volume and temperature measurements are of marginal usefulness for reasons which will be given below. The pressure measurement alone is of importance in these experiments and technological difficulties in measuring the pressure have caused several delays in this work. The signals from the transducers must be conditioned for use on a Minneapolis-Honeywell 1508 Visicorder Galvanometer Oscillograph. Biasing and expanded scale techniques have to be used to obtain the required sensitivity. A

typical oscillogram of an expansion is shown in fig. 15.

A block diagram of the pressure measuring system is given in fig. 16. The transducer is a small, solid-state, strain-gauge-type device which is mounted in the glass wall of the chamber. Its natural frequency is about 40 kc. The output is amplified by means of a potentiometric DC amplifier, also solid-state, and presented to a noise-free attenuator.

In order to obtain the required sensitivity in the pressure measurement ($\pm$ 0.5 mm. Hg), an expanded scale technique was developed. The transducer is calibrated on two scales each with its own bias voltage derived from a separate bias channel. The usual procedure is to set the pressure trace on the Visicorder near center scale for one bias with the chamber pressure near that which obtains in the ready position. This scale, called scale 1A, is calibrated against a Kollsman differential pressure gauge by bleeding small amounts of helium into and out of the chamber and recording the pressure on the Visicorder for each setting of the chamber pressure. The Kollsman gauge is corrected for atmospheric pressure each time a reading is taken.

A second pressure scale, 2A, is calibrated in the same way at lower pressures using a different bias channel. Scale 2A is biased so the Visicorder galvanometer is on scale at the pressures which prevail during the sensitive time. The relay repeater monitors the timer pulses to the valves and switches the proper bias channel

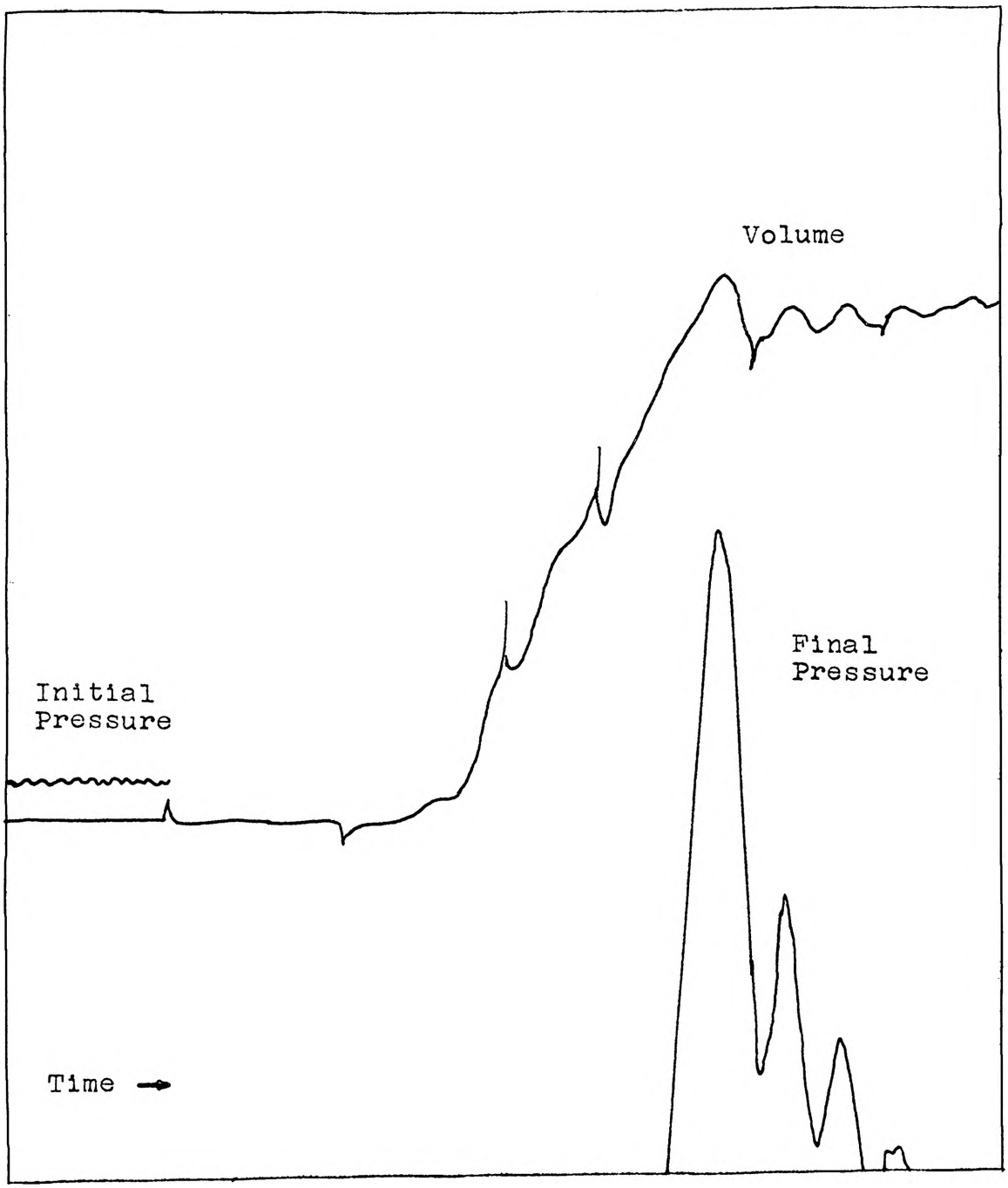

Figure 15

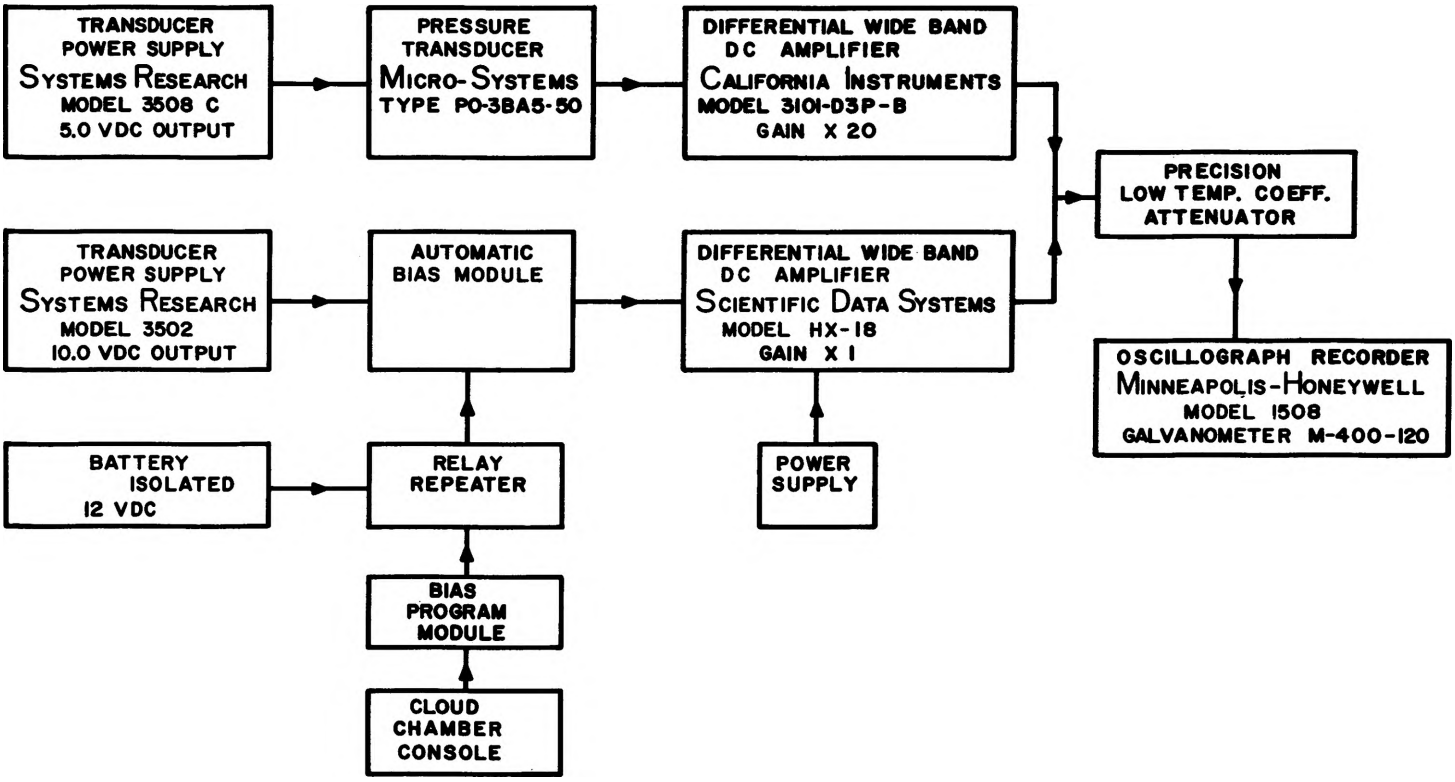
TRANSDUCER
POWER SUPPLY
SYSTEMS RESEARCH
MODEL 3508 C
5.0 VDC OUTPUT
PRESSURE
TRANSDUCER
MICRO-SYSTEMS
TYPE PO-3BA5-50
DIFFERENTIAL WIDE BAND
DC AMPLIFIER
CALIFORNIA INSTRUMENTS
MODEL 3101-D3P-B
GAIN X 20
PRECISION
LOW TEMP. COEFF.
ATTENUATOR
TRANSDUCER
POWER SUPPLY
SYSTEMS RESEARCH
MODEL 3502
10.0 VDC OUTPUT
AUTOMATIC
BIAS MODULE
DIFFERENTIAL WIDE BAND
DC AMPLIFIER
SCIENTIFIC DATA SYSTEMS
MODEL HX-18
GAIN X 1
OSCILLOGRAPH RECORDER
MINNEAPOLIS-HONEYWELL
MODEL 1508
GALVANOMETER M-400-120
BATTERY
ISOLATED
12 VDC
RELAY
REPEATER
POWER
SUPPLY
BIAS
PROGRAM
MODULE
CLOUD
CHAMBER
CONSOLE

Figure 16

into the pressure signal when the valves fire. A diode array is used to select the proper switching scheme. Common-mode voltages and 60 cycle noise have been virtually eliminated from the pressure signal by rather tedious and expensive methods of shielding, grounding and isolating.

The volume of the chamber is measured by a linear potentiometer, the movable contact of which is fastened to the piston. A DC amplifier couples the volume transducer to a separate Visicorder galvanometer. The volume transducer is relatively insensitive and, hence, is of marginal usefulness in precision work. Its primary use arises from the fact that it displays the actual chamber cycle in full detail so that the operator can see the effect of each valve visually.

A 0.0005 inch diameter chromel-alumel thermocouple monitors the temperature of the sensitive volume. Its output is amplified and then recorded by a separate galvanometer. In these experiments this thermocouple is used exclusively to monitor the pre-expansion temperature of the sensitive volume. Condensation on the thermocouple during the expansion frustrates any attempt to continuously monitor the temperature of the sensitive volume during the expansion.

6. Photographic Techniques. In order to determine the concentration of condensing droplets, N, the best high resolution photographic techniques have been used.

The sensitive volume is photographed with a stereoscopic camera which is capable of 22 stereo pairs per expansion. Two Nikon 55 mm., f/3.5 Micro-Nikkor lenses with Kodak Linagraph Shellburst 35 mm. film, ASA 400, have been found to give the best resolution commensurate with high speed and sufficient depth of focus. The object-to-film distance is approximately 53 cm. and the corresponding de-magnification is about 1/10. The film is developed in half strength Acufine Industrial developer for 23 minutes. A Nikor film processing machine is used. Typical photographs of a homogeneous nucleation and a heterogeneous nucleation are shown in plates 1 and 2 respectively.

Illumination is provided by two xenon flash lamps which are located on opposite sides of the chamber. Their beams are focused by cylindrical lenses and are collimated to give a sharply defined beam of about 2 cm. width near the center of the chamber. The lamps are triggered simultaneously and are adjusted so their beams overlap perfectly. Discharge from a 120 μfd, 2500 vdc capacitor flashes the lamps. A complicated triggering circuit shown in fig. 17 synchronizes the film advance and the flash lamps. This circuit is modified by adding a second thyratron trigger circuit to flash the second xenon flash tube. Plate 3 shows the scattering of the flash lamp beams by condensation on the chamber walls.

Chamber dimensions are correlated with the dimensions of the projected negatives by photographing a grid

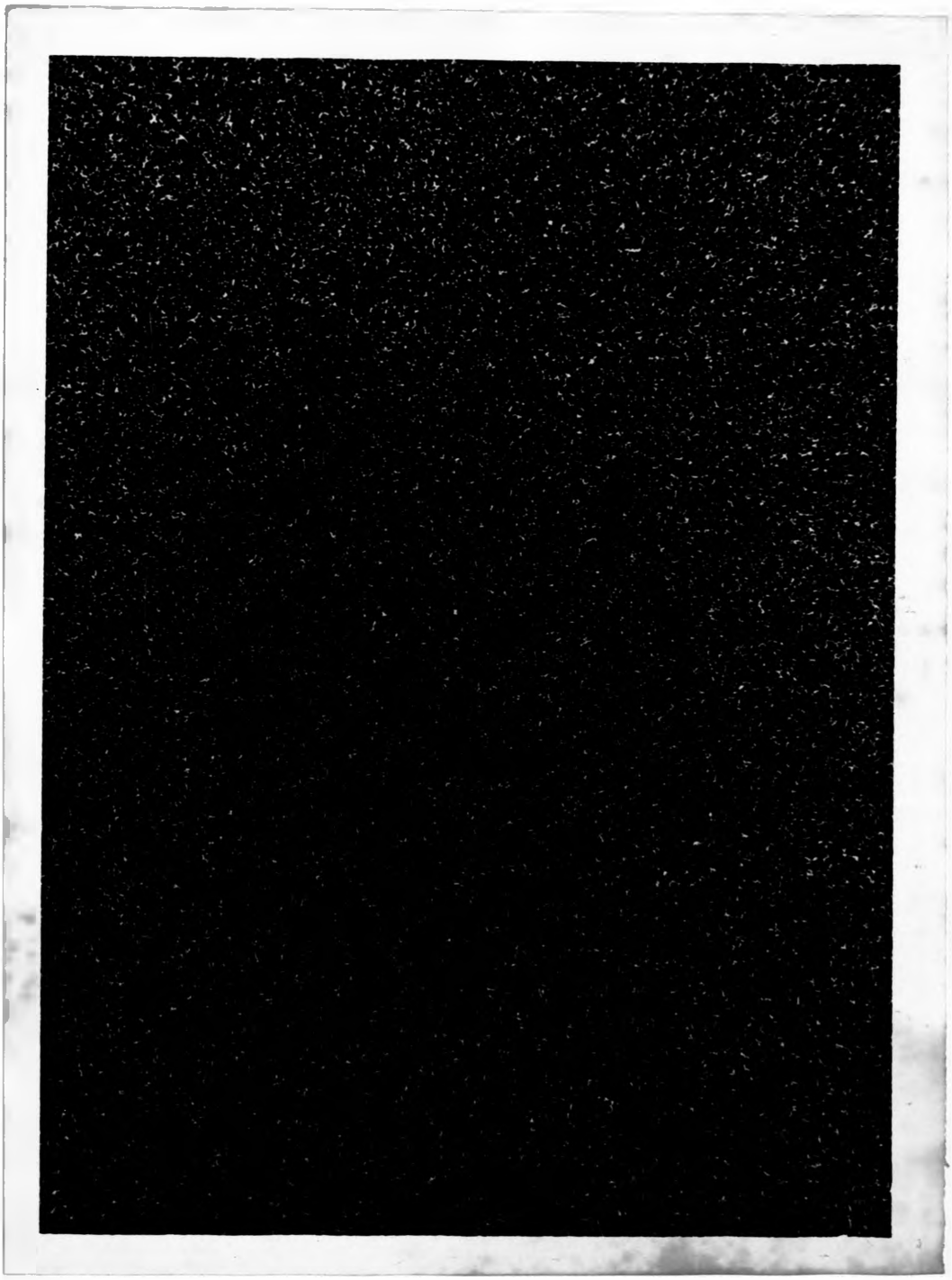

PLATE I

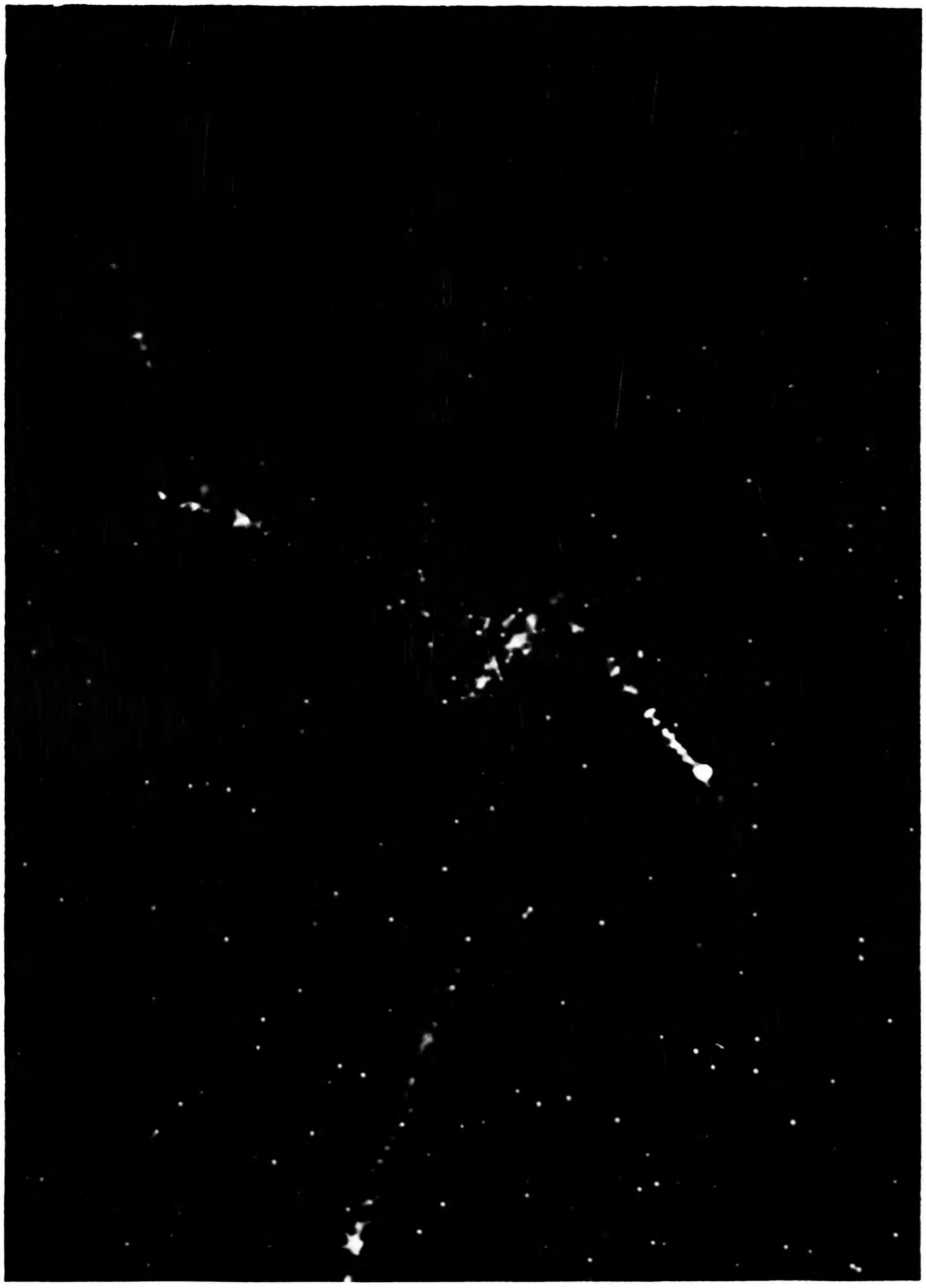

PLATE 2

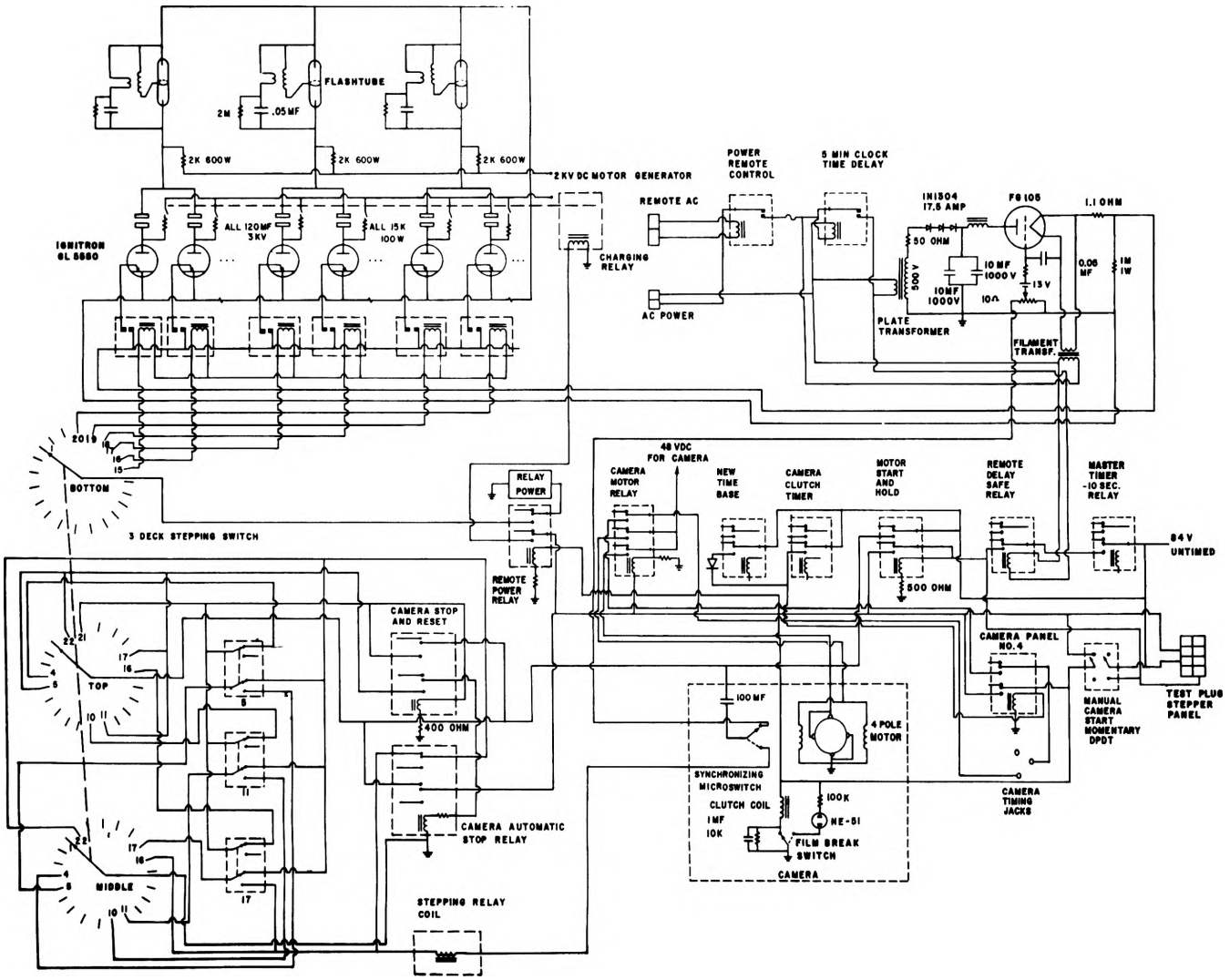
FLASHTUBE
2M
.05MF
2K 600W
2K 600W
2K 600W
2 KV DC MOTOR GENERATOR
IGNITRON GL 5550
ALL 120MF 3KV
ALL 15K 100W
CHARGING RELAY
REMOTE AC
AC POWER
POWER REMOTE CONTROL
5 MIN CLOCK TIME DELAY
IN1504 17.5 AMP
FG 105
1.1 OHM
50 OHM
10 MF 1000 V
10MF 1000V
10Ω
13 V
0.05 MF
1M 1W
500 V
PLATE TRANSFORMER
FILAMENT TRANSF.
201
BOTTOM
3 DECK STEPPING SWITCH
RELAY POWER
REMOTE POWER RELAY
48 VDC FOR CAMERA
CAMERA MOTOR RELAY
NEW TIME BASE
CAMERA CLUTCH TIMER
MOTOR START AND HOLD
REMOTE DELAY SAFE RELAY
MASTER TIMER -10 SEC. RELAY
84 V UNTIMED
600 OHM
CAMERA STOP AND RESET
400 OHM
CAMERA AUTOMATIC STOP RELAY
TOP
MIDDLE
STEPPING RELAY COIL
100 MF
4 POLE MOTOR
SYNCHRONIZING MICROSWITCH
CLUTCH COIL
1MF
10K
100K
NE-51
FILM BREAK SWITCH
CAMERA
CAMERA PANEL NO. 4
CAMERA TIMING JACKS
MANUAL CAMERA START MOMENTARY DPDT
TEST PLUG STEPPER PANEL

Figure 17

PLATE 3

of 0.0004 inch diameter wires accurately mounted in a pattern of 1 cm. squares. The grid negative is then projected and the pattern is drawn on the projection screen. The droplets are counted with this enlarged grid as a background. The width of the flash lamp beam is accurately measured and determines the third dimension. Transmission filters are used to evaluate the intensity profile of the imperfectly defined edges of the light beam.

7. Cloud Chamber Thermodynamics. Akkey problem in this work has been to calculate the supersaturation correctly to three decimal place accuracy from measurements of the initial temperature, T_A, and the initial and final pressures. This degree of accuracy is necessary in order that the experimental nucleation rates can be meaningfully compared to the various rates predicted by theory. For this reason it has been necessary to investigate the thermodynamics of the gas-vapor mixture during the cycle.

A simplifying assumption is made, namely, that the initial expansion is almost adiabatic. Furthermore, both helium and water vapor are considered as ideal gases since, at the temperatures and pressures involved in these experiments, both gases are far removed from their critical points. Under these assumptions S can be obtained from knowledge of P_A, T_A, P_B and T_B and the ideal gas adiabatic relations

$$P_A T_A^{\frac{\gamma}{1-\gamma}} = P_B T_B^{\frac{\gamma}{1-\gamma}} \qquad (3\text{-}1a)$$

$$P_A V_A^{\gamma} = P_B V_B^{\gamma} \qquad (3\text{-}1b)$$

$$T_A V_A^{\gamma-1} = T_B V_B^{\gamma-1}. \qquad (3\text{-}1c)$$

Here γ is a composite adiabatic index for the mixture and is calculated from Richarz'[28] formula,

$$1/(\gamma - 1) = 1/(\gamma_{He} - 1)P_{He}/P + 1/(\gamma_v - 1)P_v/P, \qquad (3\text{-}2)$$

where P_{He} = the partial pressure of the helium,

P_v = the partial pressure of the water vapor,

P = the total pressure of the mixture.

The nearly ideal value of γ_{He}, 1.6600, coupled with the fact that $P_{He} >> P_v$, yields values of γ near 1.6550. Such a large γ is advantageous since the supersaturation for a given magnitude of expansion is directly proportional to γ.

One further assumes that the change in the partial pressures is proportional to the change in the total pressure during the expansion. Knowing T_A, one can find the corresponding water vapor pressure, p_A, from the International Critical Tables.[29] In the expansion the total pressure decreases from P_A to P_B and so the water vapor pressure changes from p_A to p_B according to the relation

$$p_B = p_A(P_B/P_A). \qquad (3\text{-}3)$$

The pressure p_B is significantly greater than p_B', the equilibrium vapor pressure at temperature T_B. It is necessary to calculate T_B from the adiabatic relations in order to find p_B' in the Critical Tables since T_B

cannot be measured directly due to condensation on the thermocouple during the expansion. This calculation can be made from eq. (3-1a) if γ is known.

One encounters difficulties here because γ is a function of the initial temperature. Another simple calculation based on the ideal gas adiabatic relations shows that if S is desired to three decimal place accuracy and if pressures and temperatures are known to ± 0.5 mm. Hg and ± 0.05 C° respectively, then γ must be known to three decimal place accuracy also. Unfortunately information on the temperature dependence of γ in the temperature range of these experiments is not readily available. Steam Table graphs of γ vs T_A would not permit extrapolation to the desired degree of accuracy.

A way was found, however, to obtain the desired accuracy in γ_v by using a temperature-entropy diagram famaliar in engineering practice. The adiabatic index for helium was taken as 1.6600, the value at 15 °C. Figure 18 shows the temperature-entropy diagram for water vapor.[30] The vapor region isobars have been extended below the saturation line. If a temperature-entropy-pressure surface is constructed, it can be seen that the saturation curve forms the intersection of two surfaces, the liquid-vapor and the vapor surfaces. The isobar extensions overhang the liquid-vapor surface. McDonald[1] presents a clear discussion of such metastable extensions of ordinary thermodynamic surfaces and their relation to

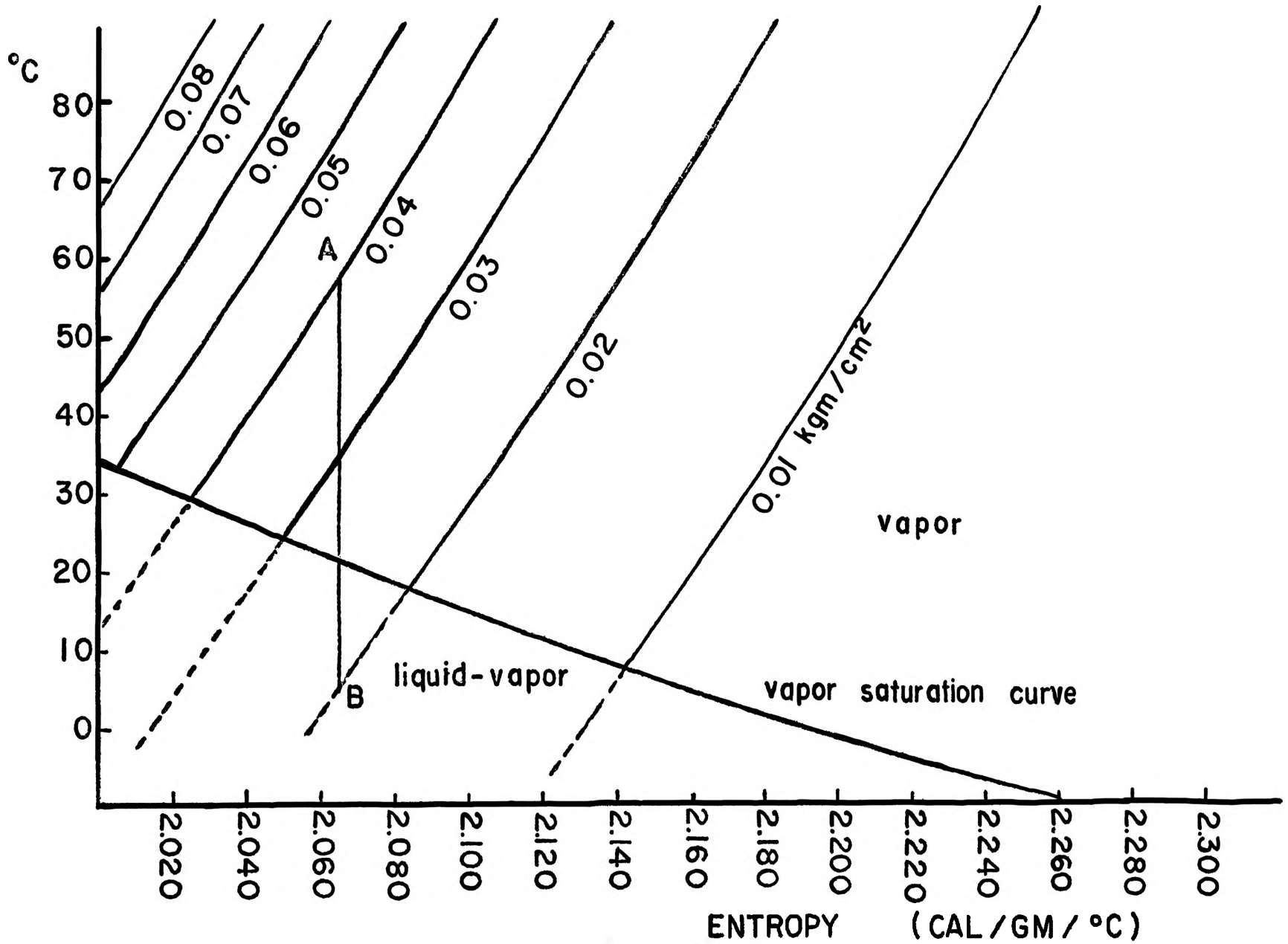
°C
80
70
60
50
40
30
20
10
0
0.08
0.07
0.06
0.05
0.04
0.03
0.02
0.01 kgm/cm²
A
B
liquid-vapor
vapor
vapor saturation curve
2.020
2.040
2.060
2.080
2.100
2.120
2.140
2.160
2.180
2.200
2.220
2.240
2.260
2.280
2.300
ENTROPY (CAL/GM/°C)

Figure 18

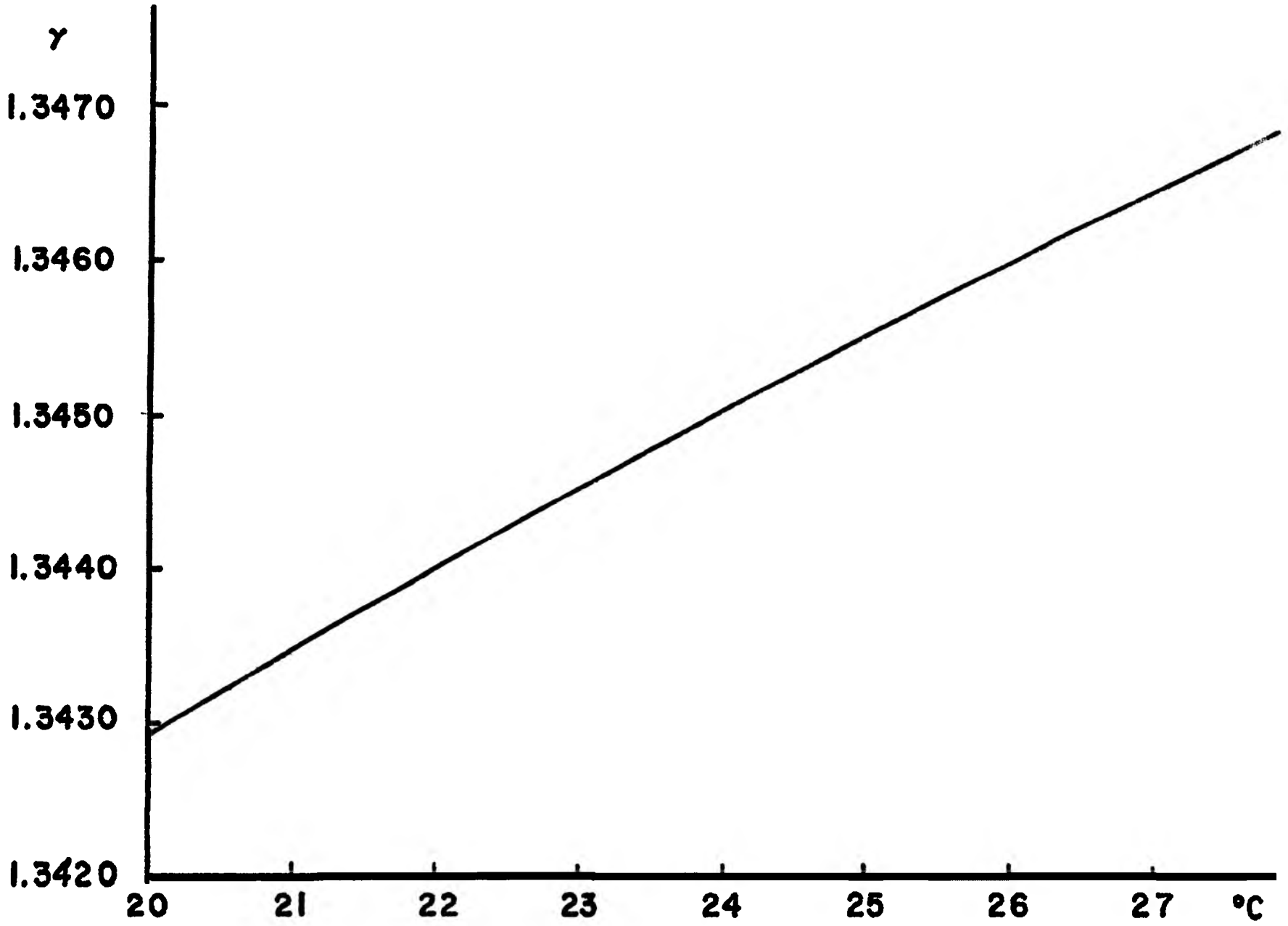

Figure 19

the condensation process. If the initial expansion is truly adiabatic and isentropic, then the central portion of the sensitive volume, considered as a subsystem of the entire sensitive volume, will move along the line of constant entropy, AB, which lies partly on the metastable extension of the vapor region surface. We assume that the water vapor does the same in its phase space so that it too undergoes an isentropic expansion. Then, since the pressure and temperature are known at two points on each isentropic curve, the adiabatic index appropriate to each curve can be found. The adiabatic index for water vapor as a function of temperature is shown in figure 19. The accuracy is to three decimal places as required.

The cloud chamber and its associated equipment offer significant advantages over the devices used by earlier researchers in the field of homogeneous condensation. It is now possible with the aid of this chamber to attempt a direct verification of the nucleation rate laws outlined in chapter II. The results of the author's homogeneous nucleation rate researches are given in the following chapter.

CHAPTER IV

AN EMPIRICAL HOMOGENEOUS NUCLEATION RATE LAW

A renewal of Allard's studies of the homogeneous nucleation rate for water vapor in helium was begun by the author in September, 1964. It is believed that significant improvements have been made in the experimental procedure and in the analysis of the data. The photographic resolution has increased five-fold over previous levels due mainly to the use of the best available optics, film and developing technique. The flash lamp beams were accurately collimated and then the intensity distribution found using transmission filters. Extreme care was taken to thermostat the liquid and the top-bottom temperature gradient as accurately as technologically possible. The error in the measurement of the sensitive time was decreased from $\pm$ 0.01 sec. in Allard's experiments to $\pm$0.001 sec. Finally, the changing condition of supersaturation which characterizes these expansions, and which was neglected in previous studies, was now taken into account.

1. Chamber Cycle. The cloud chamber is programmed as shown in fig. 20 for the homogeneous nucleation rate experiments. The cycle is identical to the one discussed

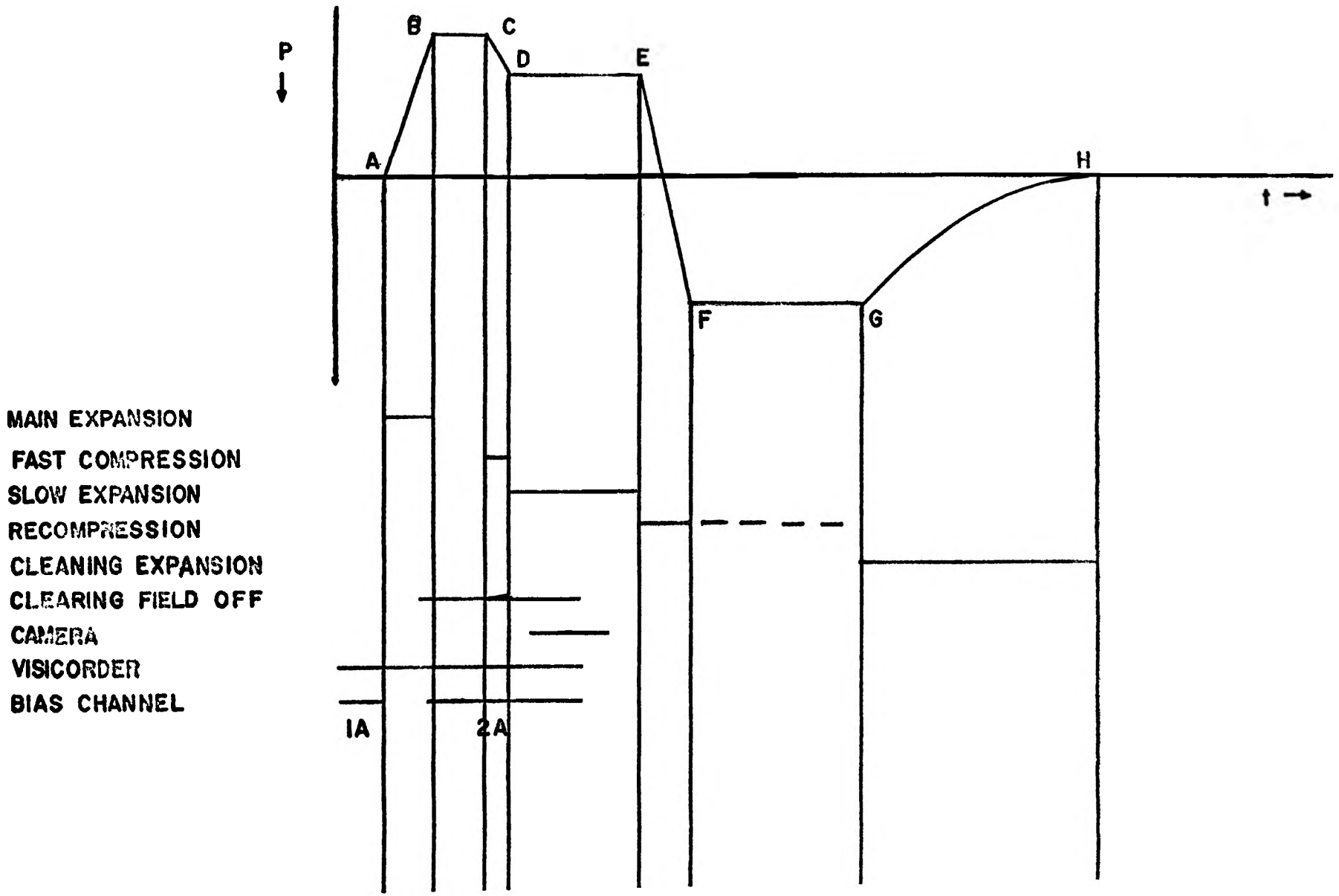
P
A
B
C
D
E
F
G
H
t
MAIN EXPANSION
FAST COMPRESSION
SLOW EXPANSION
RECOMPRESSION
CLEANING EXPANSION
CLEARING FIELD OFF
CAMERA
VISICORDER
BIAS CHANNEL
IA
2A

Figure 20

previously except for the small pulse, BCD, which is added near the end of the main expansion. The pulse provides a short sensitive time of approximately 0.03 sec. Fewer droplets nucleate during such a pulse for a given supersaturation than when the pulse is omitted and the sensitive time allowed to naturally terminate. The presence of only a few droplets allows one to investigate the homogeneous nucleation rate without the introduction of a significant error due to vapor depletion.

The pulse is produced by timing a large compression valve into the cycle a few hundreths of a second after the chamber reaches the desired level of supersaturation. The compression is rapid and of short duration causing S to decrease to slightly less than 4.2. Below S = 4.2 the nucleation rate is so low that several seconds are required for a single droplet to appear in the sensitive volume. This reduced supersaturation is still high enough to allow nuclei which formed during the pulse to grow quickly to visible size.

Ideally one would like to perform the experiment with a square pulse, i.e. one in which S is maintained constant during the sensitive time. However, the finite speed of the main expansion, AB, and the fast compression, CD, cause the pulse to assume a trapezoidal shape. In addition, piston oscillations tend to round off the top of the pulse, the net effect being to produce an

approximately parabolic-shaped pulse of nucleation (cf. fig. 15). The frequency of the oscillation is found from the oscillograms to be approximately 25 cps. The half-period of the oscillation is 0.04 sec. which indicates that, using short sensitive times of 0.03 sec., one is working entirely within the first half-cycle of the oscillation. It is evident that a time-varying S necessitates some sort of integration under the pulse in order to derive the nucleation rate law from data consisting of a recording of the pressure as a function of time and a photograph of the total population of droplets nucleated during the pulse.

The two important parameters, supersaturation and sensitive time, are easily controlled in these experiments. The peak supersaturation, which occurs at the top of the pulse, is adjusted to the desired level by varying the magnitude of the main expansion, AB. Peak supersaturations ranged from a low of 4.3 to a high of 6.2 in these experiments. The "sensitive time" is arbitrarily taken as the width of the pulse at the point where S = 4.2. Control over the length of the sensitive time, τ, is accomplished by timing the fast compression, CD, into the cycle at the desired instant. Because of the piston oscillations, a lower limit of approximately 0.025 sec. is imposed on the sensitive time.

2. Data and Analysis. Data was taken during

approximately 160 expansions on three separate days. A detailed analysis was made of 44 of these expansions. The method of analysis can perhaps be best described by means of a sample calculation based on one of the 44 expansions which were considered in detail. We shall consider expansion 103164-42 shown schematically in fig. 21. The pulse is essentially a graph of supersaturation as a function of time since each point on the pulse is associated with a unique value of S. S, in turn, is calculated from the definition

$$S = p/p_{\infty}, \tag{4-1}$$

where p is the instantaneous vapor pressure at temperature T and p_{∞} is the saturation vapor pressure over a plane surface of the liquid at the same temperature. The quantity, p, can be calculated from

$$p = p_i(P/P_i), \tag{4-2}$$

where p_i = the saturation vapor pressure at the pre-expansion temperature, T_i,

P_i = the pre-expansion total pressure,

P = the instantaneous total pressure.

Both P and P_i are directly measured during the cycle, while p_i is found from the International Critical Tables.[29] The denominator, p_{∞}, is determined from knowledge of T, the instantaneous temperature of the vapor, which is calculated, assuming adiabaticity, from

$$T = (P_i/P)^{\frac{1-\gamma}{\gamma}} T_i, \tag{4-3}$$

where γ is determined as described on p. 63 ff. Thus,

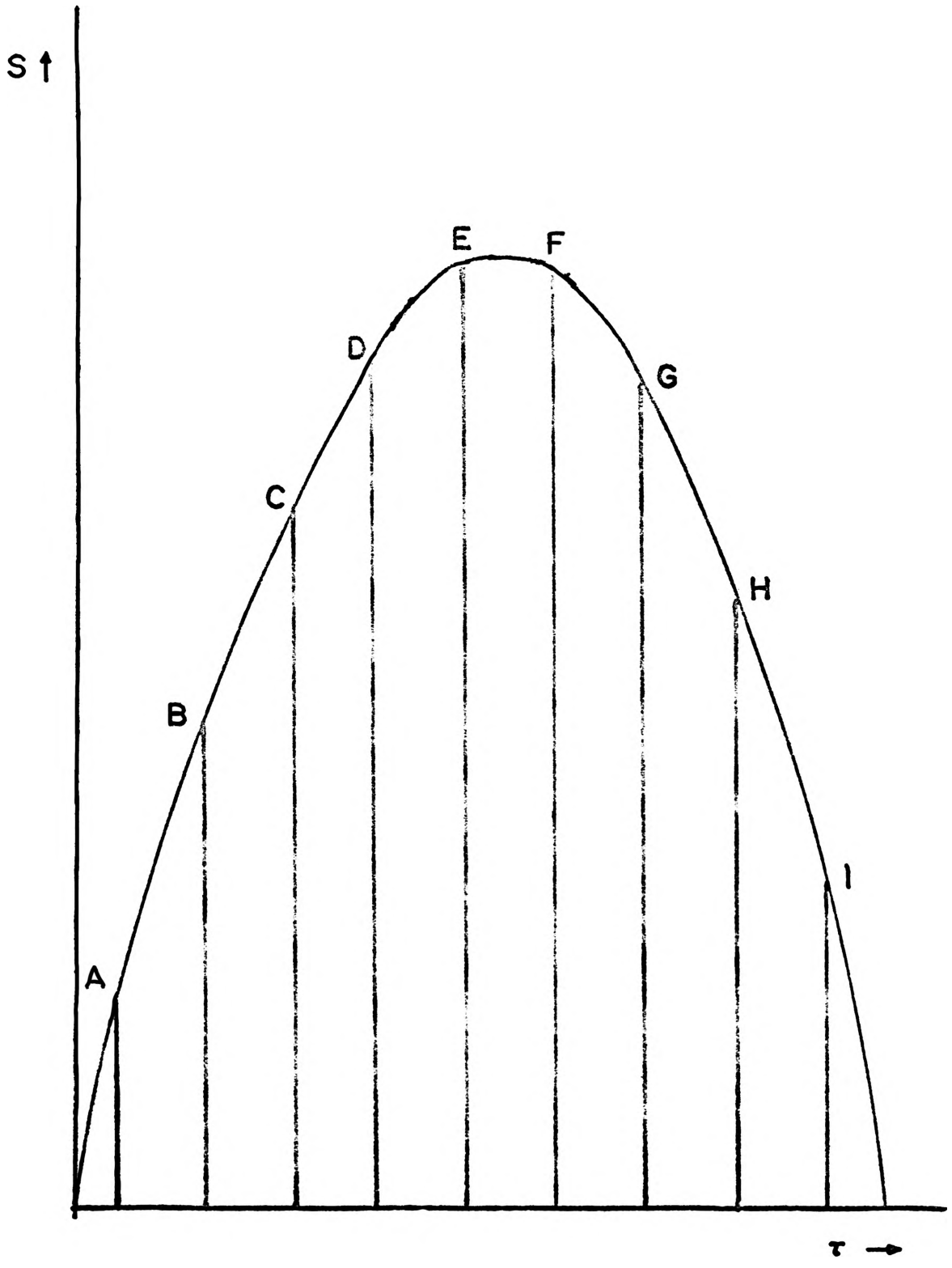

Figure 21

p_∞ is the handbook value of saturation vapor pressure at temperature T. The supersaturations found in this way apply to portions of the sensitive volume untouched by the diffusion of vapor and heat conduction.

The sensitive time is next divided into intervals of 0.005 sec. as shown in fig. 21. A average supersaturation, $\bar{S}_i$, is assumed to prevail during each interval. Then, assuming the nucleation rate law shown in fig. 22, the number of droplets nucleated during the pulse is

$$N = \sum_i \bar{J}_i \Delta t_i , \qquad (4\text{-}4)$$

where $\bar{J}_i$ is an average nucleation rate obtained from fig. 22 corresponding to $\bar{S}_i$ and $\Delta t_i = 0.005$ sec. The N calculated from eq. (4-4) should agree with the photographically observed droplet count if the appropriate nucleation rate law has been chosen. In Table II all of the pertinant data for expansion 103164-42 are given, including the analysis. The assumed nucleation rate law is adjusted until ±10% agreement is obtained for a majority of the 44 expansions. The results of the analysis using the nucleation rate law of fig. 22 is presented in Table III. Typical operating conditions for these expansions are summarized in Table IV.

The empirical nucleation rate law (cf. fig. 22) is compared to the theoretical calculations and to Allard's data (flagged points) in fig. 23. It is likely that vapor depletion effects are causing the discrepancy

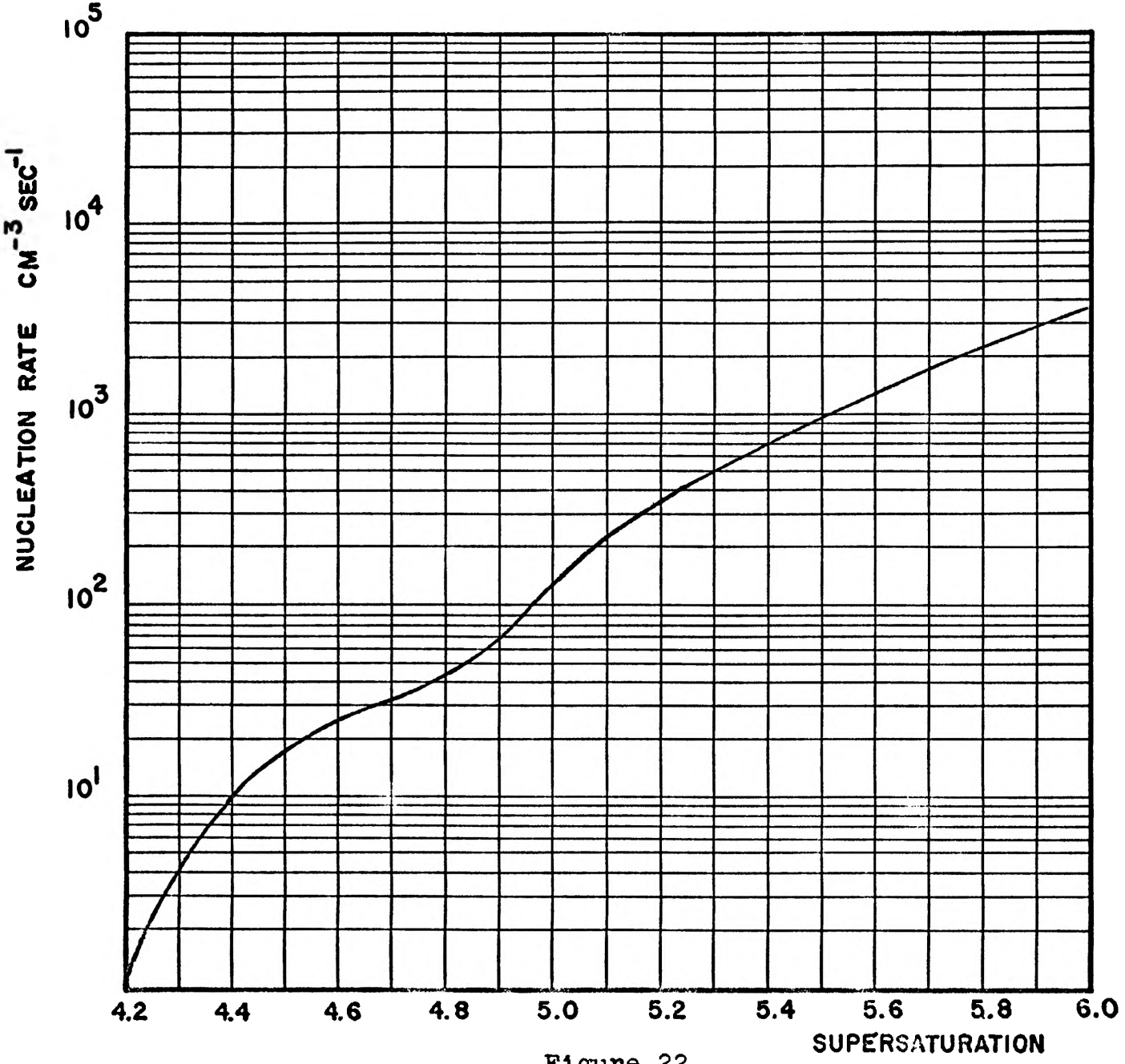
NUCLEATION RATE CM^{-3} SEC^{-1}
10^5
10^4
10^3
10^2
10^1
4.2
4.4
4.6
4.8
5.0
5.2
5.4
5.6
5.8
6.0
SUPERSATURATION

Figure 22

TABLE II

SAMPLE CALCULATION

Expansion: 103164-42

Initial temperature: 21.50 °C

Initial pressure: 643.3 inches of water

Maximum S: 5.218

Observed droplet concentration: 4.97/cm^3

Δt_i = 0.005 sec.

Pulse Analysis

Point	S	J (cm^{-3} sec^{-1})	N (cm^{-3})
A	4.267	0.04	-----
B	4.518	17.8	0.089
C	4.702	31.5	0.158
D	4.958	90.0	0.450
E	5.210	340.0	1.700
F	5.158	286.0	1.430
G	5.058	188.0	0.940
H	4.718	32.0	0.160
I	4.370	0.05	-----
			$\sum J_i \Delta t_i$ = 4.93

Per cent difference = -0.9%

TABLE III

DATA AND RESULTS

Expansion	T_1 °C	S_{max}	Droplet Count cm^{-3}	Predicted Count cm^{-3}	% Diff.
113064B-1	22.50	5.064	1.91	1.63	-14.6
103164-13	21.50	5.038	2.78	2.90	+4.4
103164-18	21.50	5.074	3.14	2.84	-9.5
103164-25	21.50	5.158	2.99	3.15	+5.5
113064B-4	22.50	5.188	2.95	3.01	+2.0
113064A-7	22.75	5.218	4.52	4.83	+6.8
103164-14	21.50	5.216	3.35	3.26	-3.8
113064B-12	22.50	5.159	2.49	2.88	+15.6
103164-42	21.50	5.218	4.97	4.93	-0.9
113064B-5	22.50	5.288	5.53	5.82	+5.2
113064A-8	22.75	5.328	6.81	6.27	-8.5
113064B-7	22.50	5.422	7.14	8.09	+13.4
113064B-14	22.50	5.395	6.93	6.98	+0.7
113064B-8	22.50	5.421	7.95	7.46	-6.2
113064A-3	22.75	5.462	8.72	8.83	+1.3
113064A-2	22.75	5.500	9.71	10.86	+11.9
113064A-11	22.75	5.580	13.87	12.44	-10.3
111664B-9	22.00	4.575	0.35	0.37	+5.7
103164-21	21.50	4.540	0.27	0.25	-7.4
103164-26	21.50	4.570	0.36	0.31	-13.9
103164-38	21.50	4.548	0.38	0.36	-5.3
111664B-10	22.00	4.575	0.46	0.42	-8.7
103164-15	21.50	5.590	15.67	16.92	+8.0
103164-17	21.50	5.534	12.04	12.04	0.0
113064B-15	22.50	5.676	15.05	16.26	+8.0
113064B-13	22.50	6.121	70.70	67.90	-3.9
113064B-20	22.50	6.177	87.00	84.80	-2.5
113064B-19	22.50	5.882	32.00	35.97	+12.4
113064B-18	22.50	5.929	40.25	40.06	-0.5
113064B-10	22.50	5.816	28.70	28.70	0.0
113064B-17	22.50	5.784	23.55	27.45	-16.5
113064B-16	22.50	5.748	25.00	24.28	-2.9
113064B-11	22.50	5.750	20.00	22.70	+13.5
103164-41	21.50	4.860	1.03	1.03	0.0
103164-12	21.50	4.932	1.12	0.87	-22.3
103164-40	21.50	4.730	0.64	0.60	-6.7
103164-43	21.50	4.614	0.40	0.41	+2.5
103164-23	21.50	4.818	0.93	0;81	-13.4
103164-19	21.50	4.996	1.53	1.65	+7.6
113064A-24	22.75	4.970	0.93	1.04	+10.6
103164-39	21.50	4.730	0.67	0.62	-8.1
103164-46	21.50	4.935	0.88	0.91	+3.0
103164-24	21.50	4.930	1.00	0.96	-4.3
103164-20	21.50	4.930	0.99	0.90	-9.2

TABLE IV

OPERATING CONDITIONS

1. Chamber Constituents

Liquid: demineralized, distilled water blackened with Putnam dye.
Inert gas: Helium (Matheson Company).

2. Temperatures

Room temperature: 18.5 °C.
Reference bath: 23.50 °C.
Top-bottom gradient: 0.50 °C.
Liquid temperature: 22.50 °C.

3. Typical Sensitive Volume Pressures

Initial pressure before expansion: 645 in. water.
Fully expanded pressure: 505 in. water.
Overcompressed: 76 cm. Hg gauge in lower chamber.

4. Clearing Field

1200 volts dc, 0.5 microamperes.

5. Cycle Time

4 minutes, 53 seconds.

6. Typical Valve Time Settings

Timer		Start	Stop
1	(large expansion valve)	0.15 s	0.29 s
2	(pressure scale 1A)	0.26	0.58
10	(large compression valve)	0.31	0.34
4	((small expansion valve)	0.37	1.52
5	(small expansion valve)	0.63	2.54
7	(recompression)	6.20	52.50

7. Illumination

Incandescent: 200 vac, 10 amps with a glass filter and $CuSO_4$ solution filter.
Flash: 2 xenon flash tubes, 3/8 in. dia., 10 in. long.
360 degrees aluminized with 1/8 in. slit made by hand.
1900 vdc.
Kodak 8K2 ultraviolet filter.

8. Photography

Stereo movie camera, 35 mm. Two 55 mm. f/3.5 Nikon Micro-Nikkor lenses.
Operating voltage: 52 vdc, 10 amps.
Aperture: f/5.6 or f/8.0 depending of whether one or two lamps were used per exposure.
Object-to-film distance: 53 cm.
Depth of focus: 5 cm.
De-magnification: 1/10.
Framing rate: 10/sec.

9. Film Processing

Kodak Linagraph Shellburst film and Kodak Tri-X Pan.
Developer: Acufine Industrial, 23 min., 1-1 dilution at room temperature.
Stop bath: 1 min.
Fixer: General Electric Liquid X-ray fixer, 17 min.
Washing: 30 min. in running tap water.
Each batch of developer was used for 200 feet of film and then discarded.

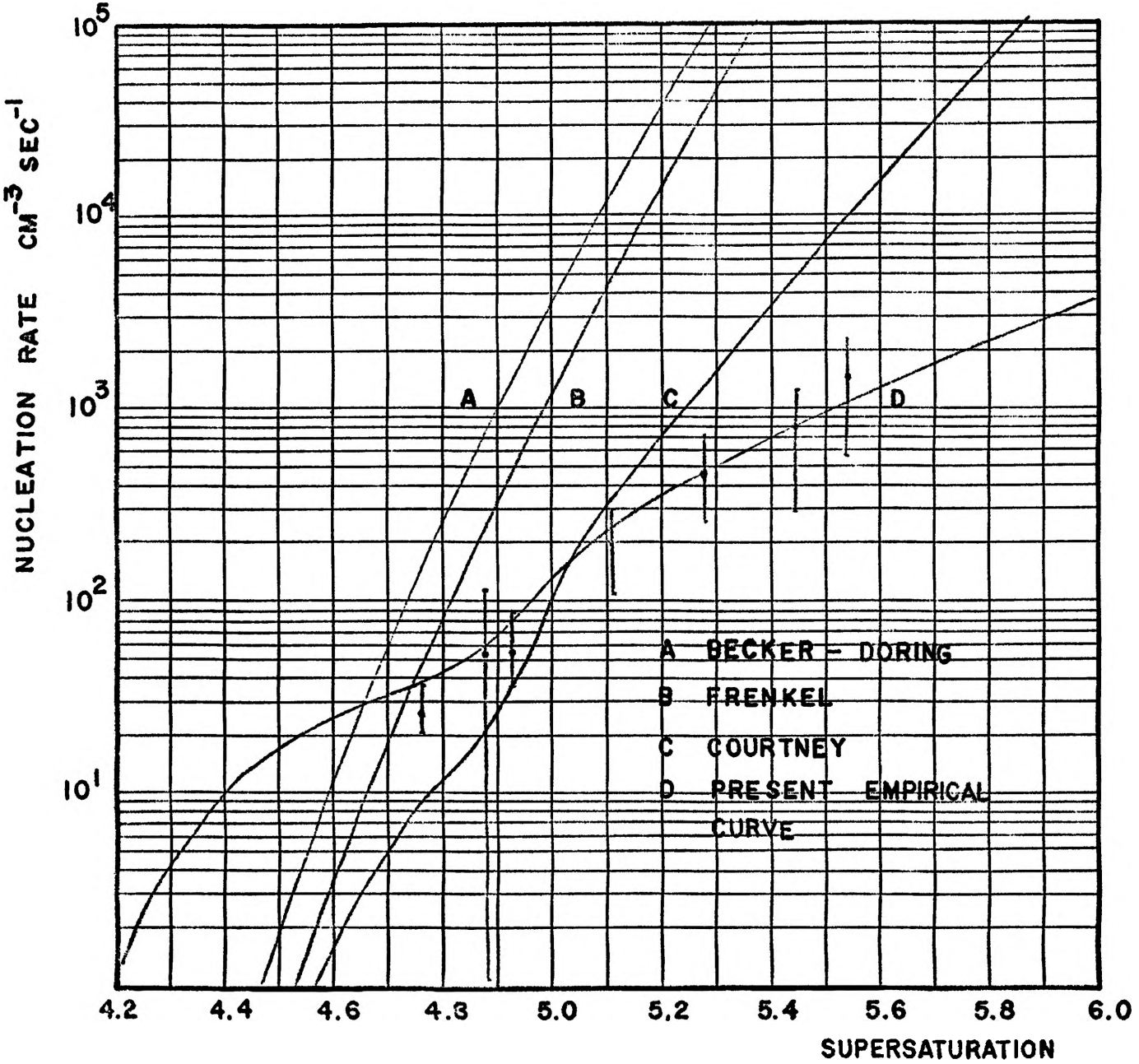
NUCLEATION RATE CM^{-3} SEC^{-1}
10^5
10^4
10^3
10^2
10^1
A
B
C
D
A BECKER – DORING
B FRENKEL
C COURTNEY
D PRESENT EMPIRICAL CURVE
4.2
4.4
4.6
4.8
5.0
5.2
5.4
5.6
5.8
6.0
SUPERSATURATION

Figure 23

between curves C and D in the range $S > 5.4$. The droplet concentrations varied from $15/cm^3$ to $100/cm^3$ for an increase in S from 5.2 to 6.2. Courtney's vapor depletion calculation relies on the Frenkel rate law which predicts rates that are much too high for this particular range of supersaturations. It is likely that Courtney's collision-frequency growth law gives an unrealistically high rate of growth for the droplets. Actually, collision-frequency should provide the fastest growth rates (and, hence, the fastest rate of vapor depletion) which makes it difficult to explain the large rates predicted by curve C for $S > 5.4$. One concludes that the Frenkel rate law is much too high. This result is expected since Frenkel takes no account of vapor depletion in his calculation. The use of shorter sensitive times would lessen the effects of vapor depletion on the nucleation rate. However, the response of the apparatus limits the speed of the expansions and compressions.

The relatively high rates predicted by curve D for $S < 4.7$ indicates the possibility that background nucleation is noticably altering the rates. The highest droplet concentrations for these supersaturations is approximately $0.6/cm^3$. The typical background level for these experiments is 1 droplet/50 cm^3. This concentration is high enough to cause discrepancies in the droplet counts for peak supersaturations below

4.5.

3. Estimation of Accuracy. It is difficult to calculate the effects of errors in S, J and τ on the experimental results except in an idealized situation in which the nucleation pulse is assumed to be parabolic and the nucleation rate law is a simple logrithmic function (cf. fig. 24). The pulse can be written as

$$S = At^2, \tag{4-5}$$

where S = S - 4.200. Considering a symmetrical pulse of width 0.03 sec. at S = 4.200 as typical of our expansions, A is given by

$$A = (4.4 \times 10^3)\,\hat{S}, \tag{4-6}$$

where $\hat{S}$ is the peak value of supersaturation for the pulse. The linear nucleation rate law which fits curve D, fig. 23 is

$$J = 5.3 \exp[(0.554)S]$$
$$= 5.3 \exp[(2.46 \times 10^3)\hat{S}\, t^2]. \tag{4-7}$$

The relative error in J, assuming that the error in t, t, is $\pm 10^{-3}$ sec., is then

$$\delta J/J = 0.15\,\hat{S}. \tag{4-8}$$

For a peak S of 5.00, $\delta J/J = \pm 0.12$, or, in terms of per cent error, ± 12%. The corresponding error in S is estimated to be ± 0.01 based on the error analysis given by Allard.[10] A further error can be introduced in the process of droplet counting and has been assumed to be $\pm N^{1/2}$, where N is the total number of droplets counted either in a single expansion or in several identical

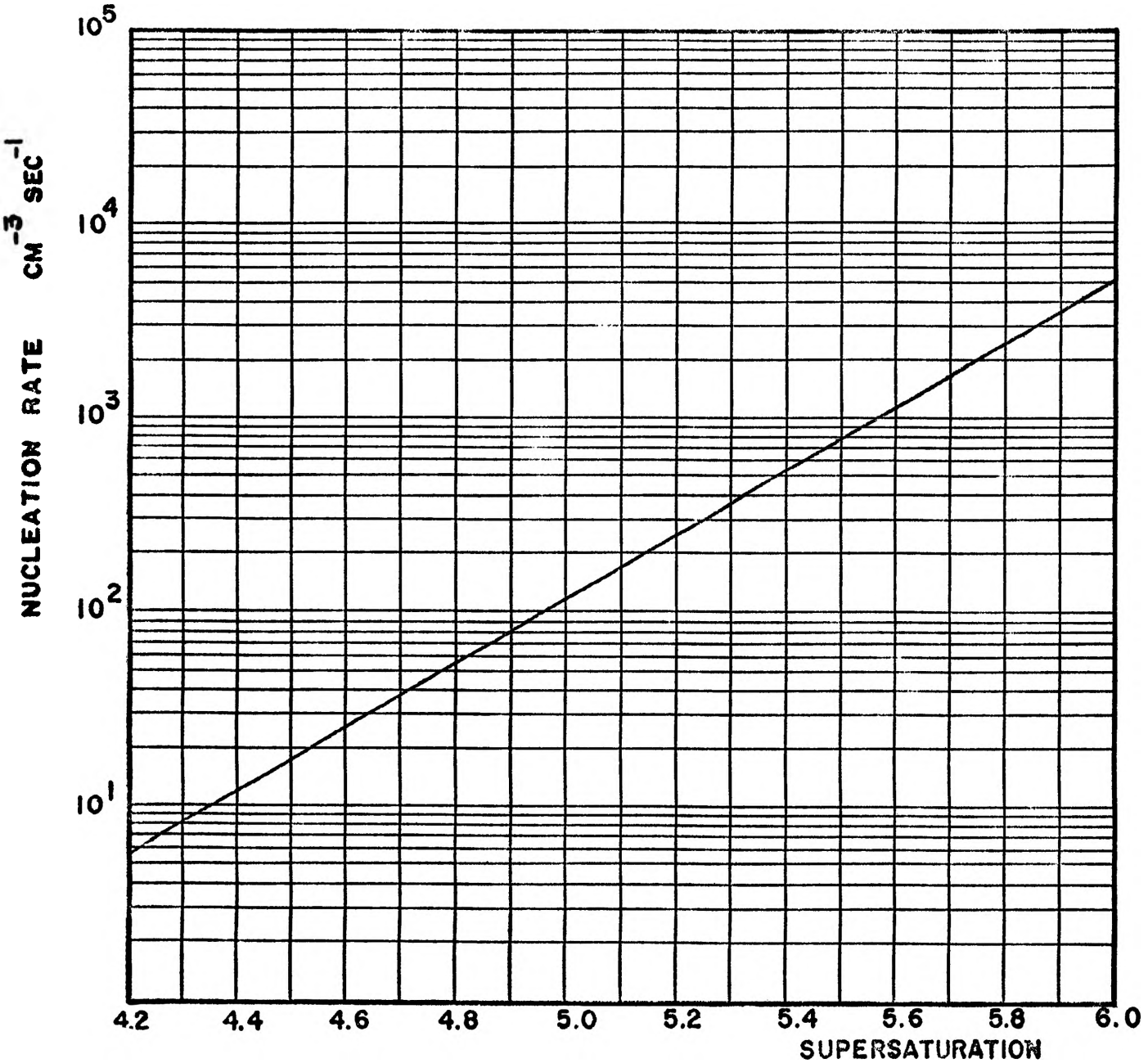
NUCLEATION RATE CM^{-3} SEC^{-1}
10^5
10^4
10^3
10^2
10^1
4.2
4.4
4.6
4.8
5.0
5.2
5.4
5.6
5.8
6.0
SUPERSATURATION

Figure 24

expansions. N is typically on the order of 100 droplets. This yields a relative counting error of about ± 10%. An estimation of the corresponding error in J can be obtained by considering an average nucleation rate, $\bar{J}$, such that for the expansion

$$N = \bar{J} V \tau, \qquad (4\text{-}9)$$

where τ = the sensitive time,

V = the total volume counted.

The relative error in V, $\delta V/V$, is approximately $\pm 2.8 \times 10^{-2}$ cm^3. Then, if $\tau = 0.03$ sec. and $\delta\tau = \pm 10^{-3}$ sec., a simple calculation yields

$$\delta\bar{J}/\bar{J} = 1/N \, (\delta N - \delta\tau/\tau - \delta V/V)$$
$$= 1/N \, (N^{1/2} - 0.0033 - 0.0028/V). \qquad (4\text{-}10)$$

5. Future Work. It is clear from this study of homogeneous condensation that vapor depletion effects cannot be ignored for high supersaturations ($S > 5.2$) even for short sensitive times of 0.03 sec. To obtain shorter sensitive times would necessitate a major redesigning of the chamber, the valving and the electronic circuitry. A new chamber is presently under construction and will feature several innovations designed to remove the piston oscillations and thus allow longer sensitive times unaffected by oscillations. Studies have been initiated to provide a quantitative measure of the vapor depletion effect by making use of the inherent oscillations in the chamber. Hopefully an estimation of the rate of growth of the dead spaces around the growing

droplet will emerge from these studies. With such knowledge one can begin to find corrections to the newly found empirical rate law. Such corrections are expected to shift the rate law towards higher rates in the region $S > 5.2$. This effort will require an uncommonly high degree of purity in the chamber gas and in the liquid. Chamber impurities tend to lower the surface free energy of the embryos and cause condensation to proceed more efficiently. It is clear that surface phenomena play a crucial, and as yet little understood, role in the condensation process.

Large electrostatic fields were observed to produce a strange condensation effect, perhaps due to the very high fields present at point projections on the clearing field wires. Plate 4 shows this anomaly which was observed when the potential difference between the clearing field wires and the liquid was 2300 volts. The two clouds, which resemble cigarette smoke in the initial stages of their growth, are composed of numerous fine droplets originating near the clearing field wire (which appears as a faint line near the top of the photograph). Plate 5 is an enlargement of the smaller cloud. The droplets are too small to be clearly resolved in the photographs. Abnormally high clearing field currents, which pegged a 20 μamp meter, were observed at the time these clouds appeared. The cloud of droplets is evidently highly charged and tends to

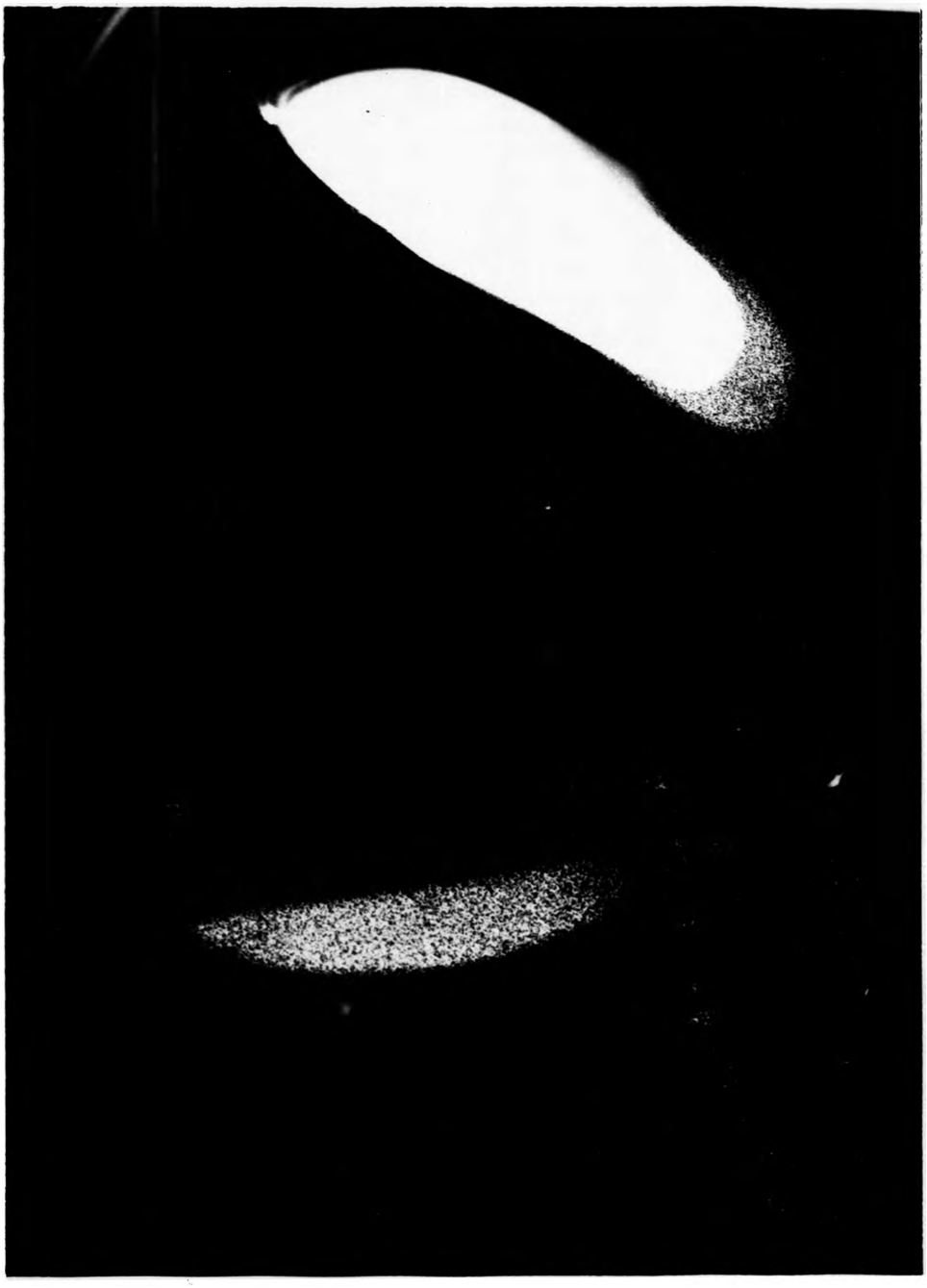

PLATE 4

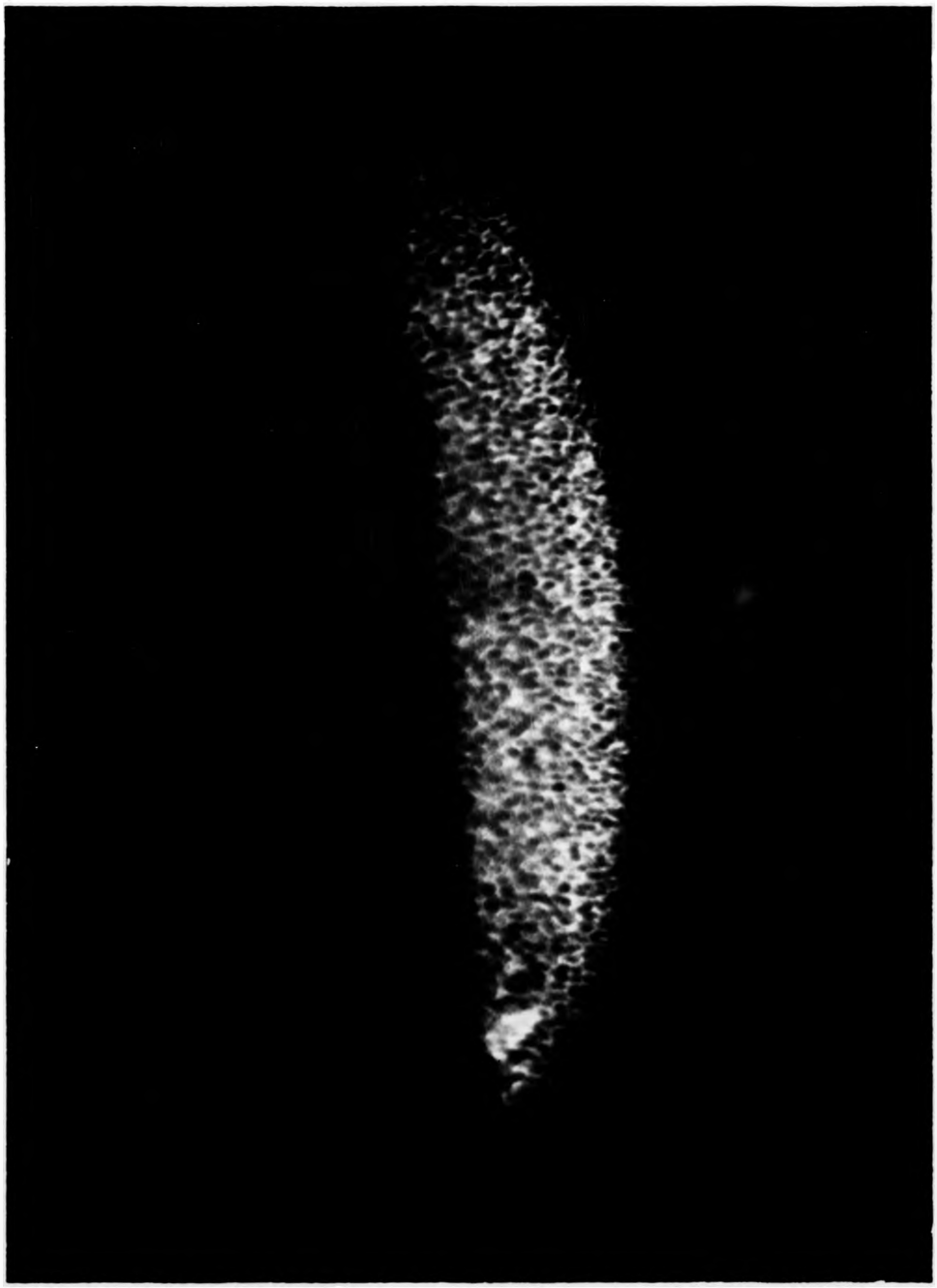

PLATE 5

move along the field lines. It is possible that they are manifestations of a form of electrical spraying[31] caused by a very high electric field associated with a sharp point on the clearing field wires. The effect disappears when the potential difference between the clearing field electrodes is decreased to 1300 volts. This behavior indicates that there may exist a critical supersaturation for the appearance of the phenomenon in a given electrostatic field. Perhaps a form of condensation discharge, resembling corona discharge, is occurring in the presence of large supersaturations. It is possible that such a mechanism could be responsible for a major portion of the corona-type discharge from trees and other vegetation on the earth's surface. The effect should be studied in detail to determine the validity of these ideas.

Finally, the problem of vapor density gradients in the chamber has not been adequately investigated to date. Plate 6 shows a very inhomogeneous concentration of droplets which was traced to the presence of condensation on one part of the chamber walls. The presence of thermal gradients in the chamber may give rise to vapor density gradients which, in turn, could produce uneven conditions of supersaturation when the chamber expands. Our present assumption is that saturated conditions prevail throughout the chamber immediately before expansion. Edge effects are eliminated since only the

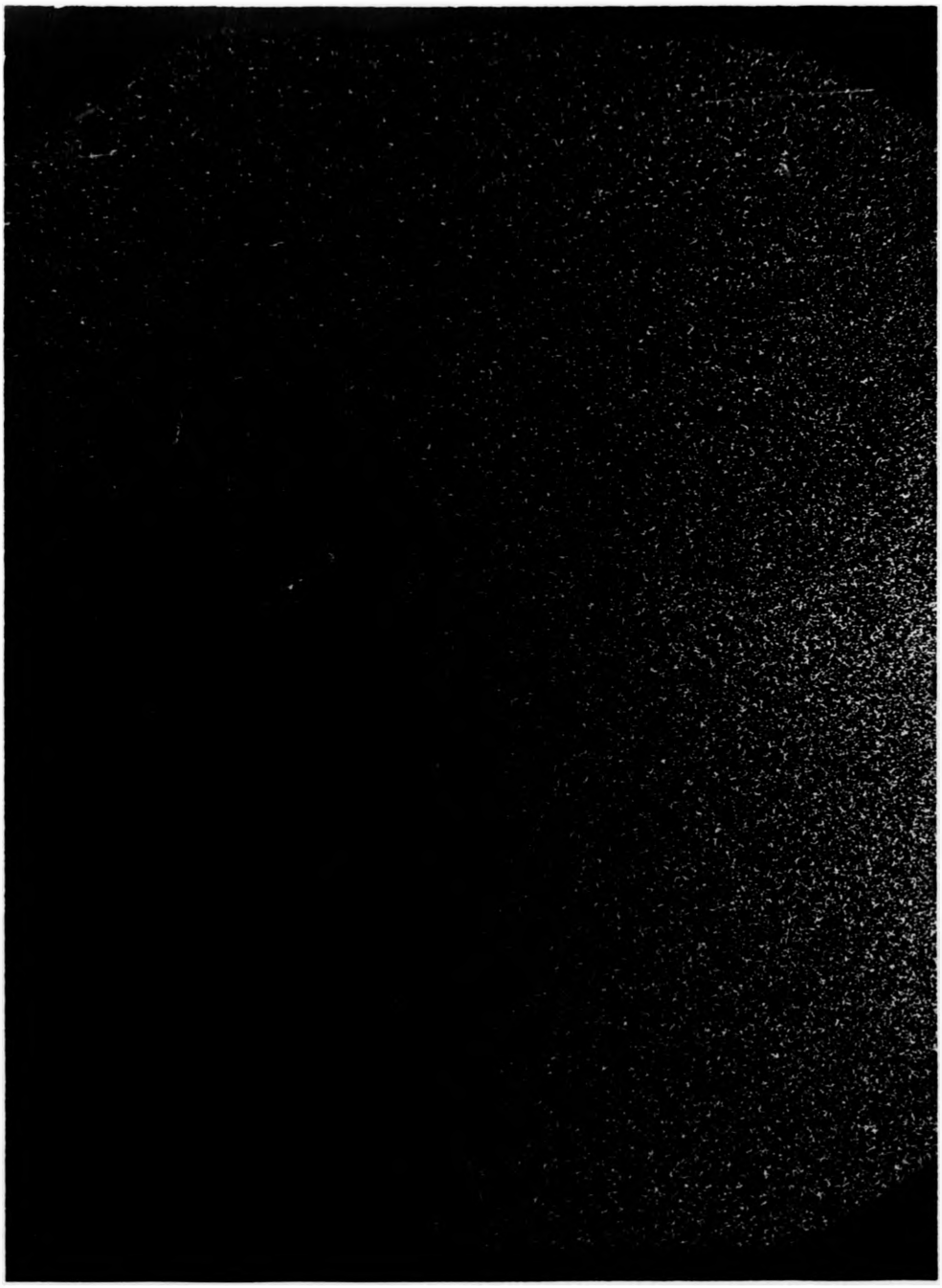

PLATE 6

center of the chamber was observed photographically.

5. Summary. The primary objective of this work was to improve the technique, first developed by Allard, for measuring homogeneous nucleation rates. The photography was greatly improved yielding higher and more uniform resolution throughout the entire depth of field. Greater control was established over the liquid temperature and the top-bottom gradient rather than relying on room temperature to establish these parameters. The noise level in the critical pressure measurement was significantly reduced. The pressure system amplifier was changed from the differential to the potentiometric mode of operation in order to achieve greater stability. An unsuccessful attempt was made to eliminate mechanical oscillations following compressions and expansions. However, a means of employing these oscillations to advantage was developed. Temperature-entropy diagrams, constructed from a modified van der Waals equation of state which takes clustering into account, was used to calculate reliable values for the adiabatic index of water vapor at the temperatures employed in these researches. Previously, data for 100 ^{o}C was used. An integration technique was utilized to analyze the pulses of nucleation. This procedure allows one to take into account the presence of time-varying supersaturations in these expansions.

BIBLIOGRAPHY

1. J. D. McDonald, "Homogeneous Nucleation of Vapor Condensation I, Thermodynamic Aspects," Am. Jour. of Phys. 30, 870 (1962).

2. W. G. Courtney, Kinetics of Condensation from the Vapor Phase, Summary Report TM-1250, Texaco Experiment, Inc., 1961.

3. B. J. Mason, "Spontaneous Condensation of Water Vapor in Expansion Chamber Experiments," Proc. Phys. Soc. B64, 773 (1951).

4. R. Becker and W. Döring, "Kinetics of Nucleation in Supersaturated Vapors," Ann. der Physik 24, 719 (1935).

5. J. Frenkel, Kinetic Theory of Liquids, New York: Dover Publications, Inc., 1955.

6. J. Zeldovich, "Theory of the Formation of a New Phase," J. Exp. Theor. Phys. (Russian) 12, 525 (1942).

7. F. J. M. Farley, "The Theory of Condensation of Supersaturated Ion-free Vapor," Proc. Roy. Soc. A212, 530 (1952).

8. C. T. R. Wilson, "Condensation of Water Vapor in the Presence of Dust-free Air and Other Gases," Phil. Trans. Roy. Soc. (London) A189, 265 (1897).

9. N. K. Das Gupta and S. K. Ghosh, "A Report on the Wilson Cloud Chamber and Its Applications in Physics," Rev. Mod. Phys. 18, 225 (1946).

10. E. F. Allard, "A New Determination of the Homogeneous Nucleation Rate of Water in Helium," Ph.D. Dissertation University of Missouri at Rolla, 1964.

11. F. Frey, "On the Condensation of Vapor in an Inert Gas," Z. Phys. Chem. B49, 83 (1941).

12. J. L. Kassner and E. F. Allard, "A New Cloud Chamber Method for the Determination of Homogeneous Nucleation Rates," To appear in the Jour. Chem. Phys., Feb., 1965.

13. J. G. Wilson, The Principles of Cloud-Chamber Technique, Cambridge: University Press, 1951.

14. C. F. Powell, "Condensation Phenomena at Different Temperatures," Proc. Roy. Soc. A119, 553,(1928).

15. E. J. Williams, "Note on the Sensitive Time of a Wilson Cloud Chamber," Proc. Camb. Phil. Soc. 35, 512 (1939).

16. H. Reiss, "The Kinetics of Phase Transitions in Binary Systems," J. Chem. Phys. 18, 840 (1950).

17. J. W. Gibbs, The Collected Works of J. W. Gibbs, New York: Longmans, Green and Co., 1948.

18. J. H. Keenan, Thermodynamics, New York: John Wiley and Sons, Inc., 1941, chapters 24-26.

19. G. M. Pound, L. A. Madonna and C. M. Scuilli, "Low Temperature Cloud Chamber Studies on Water Vapor," Proc. of the Conference on Interfacial Phenomena and Nucleation (Air Force Cambridge Research Center) 1955, vol. 1, p. 85.

20. M. Volmer and H. Flood, "Nucleation in Vapors," Z. Phys. Chem. A170, 273 (1934).

21. L. Farkas, "Speed of Nucleus Formation in Supersaturated Vapor," Z. Phys. Chem. 125, 236 (1927).

22. D. ter Haar, Elements of Statistical Mechanics, New York: Holt, Rinehart and Winston, 1961.

23. Lord Kelvin, "On the Equilibrium of Vapor at a Curved Surface of Liquid," Proc. Roy. Soc. Edin. 7, 63 (1870).

24. Matheson Gas Data Book, East Rutherford, New Jersey: The Matheson Company, Inc., 1961.

25. N. K. Adam, The Physics and Chemistry of Surfaces, London: Oxford University Press, 1941.

26. A. Sander and G. Kamköhler, "Supersaturation with Spontaneous Nucleation of Water Vapor," Naturwissen. 31, 460 (1943).

27. D. L. Packwood, Masters thesis, University of Missouri at Rolla, 1965.

28. F. Richarz, "The Value of the Ratio of Specific Heats for a Mixture of Two Gases," Ann. der Physik 19, 639 (1906).

29. International Critical Tables of Numerical Data, Physics, Chemistry and Technology, New York: McGraw-Hill Book Company, Inc., 1926.

30. M. P. Vukalovitch, Thermodynamic Properties of Water and Steam, Moscow: State Publishing House of Scientific-Technical Literature Concerning Mechanical Engineering, 1958.

31. R. S. Carson, "Electrical Spraying of Macroscopic Liquid Particles Under Pulsed Conditions," Ph.D. Dissertation, University of Illinois, 1964.

VITA

Raymond J. Schmitt was born Nov. 3, 1941 in St. Louis, Missouri, the eldest son of Mr. and Mrs. R. A. Schmitt. He received his elementary and high school education from parochial schools in St. Louis, Missouri. He was graduated from St. Mary's High School in June, 1959.

He entered St. Louis University, St. Louis, Missouri, in September, 1959 on a four-year academic scholarship. He received his B.S. degree in Physics from St. Louis University in June, 1959.

He entered the Graduate School of the University of Missouri at Rolla in September, 1963 as a candidate for the degree of Master of Science in Physics.